Design of the Efficient Plasmon Assisted Photocatalysts and their Application in Visible Photocatalytic Wastewater Treatment

Report to the
WATER RESEARCH COMMISSION

by

THANDEKILE MTHETHWA & JENNY LUMBALA CHANSA

Cape Peninsula University of Technology

WRC Report No. 2775/1/19
ISBN 978-0-6392-0111-5

February 2020

WATER
RESEARCH
COMMISSION

Obtainable from
Water Research Commission
Private Bag X03
GEZINA, 0031

orders@wrc.org.za or download from www.wrc.org.za

EXECUTIVE SUMMARY

Plasmonic photocatalysis has demonstrated a substantial ability in visible light utilization for environmental and energy applications. The ability of plasmonic noble metals to concentrate and scatter visible light makes them the material of choice for solar energy harvesting application. By manipulating the size or shape of metal nanostructures their plasmonic resonant wavelength can be tuned to exploit the entire solar spectrum. In recent years, it has been shown that incorporation of plasmon metals into wide band gap semiconductors can significantly improve the photocatalytic activity under visible-light spectrum. Although, TiO_2 does not typically show any photoactivity under visible light irradiation, studies have shown that when TiO_2 is coupled with metal nanoparticles it exhibits photocatalytic activity under visible light.

The aim of this work was to prepare and characterize Au/TiO_2 photocatalysts and study the photocatalytic degradation of the model textile dyes.

In view of improving TiO_2 photoefficiency under visible light, different strategies have been developed including surface plasmon sensitization. Therefore, the preparation of the visible light active photocatalysts was very crucial. In this project, gold nanoparticles (spherical and rod-shaped) were chosen to provide plasmonic properties in TiO_2 photocatalyst. Gold nanoparticles were first synthesized on their own using the well-known seed-mediated and Turkevich methods. The colloidal nanoparticles were characterized using UV-Vis spectrophotometer and Transmission electron microscopy (TEM). For the synthesis of Au/TiO_2 composites, a nucleation and growth method was adopted. TiO_2 was coated on the surface of the already prepared gold nanoparticles at 95°C for 5 hrs. UV-Vis spectrophotometer, TEM, and XRD were used to characterize the collected powder samples.

The obtained Au/TiO_2 samples were then used for degrading model azo dyes. In this project, we have demonstrated successful synthesis of visible light active Au/TiO_2 photocatalysts. Au/TiO_2 photocatalysts exhibit significant photoactivity under visible light irradiation for the degradation of azo dyes. Photodegradation results visible light demonstrated that the incorporation of gold nanoparticles significantly increases the degradation efficiency by promoting the charge carrier separation. AuNRs/TiO_2 photocatalyst presented higher photodegradation efficiency for CR compared to AuNS/TiO_2, this was due to the stronger magnetic field created by nanorods as a result of the photon absorption from both the transverse and longitudinal peaks. The reusability of the photocatalysts was also tested and they demonstrated good stability.

The results also showed the removal of colour during photodegradation, therefore, the results obtained are very promising for the treatment of textile effluents. Moreover, this project demonstrated that plasmonic photocatalysts could be used under direct sunlight. Ultimately, we hope this project could stimulate the further design of sunlight responsive materials at a larger scale.

PROJECT APPROACH

In this work, we present a simple plasmon-based photocatalyst that is able to effectively absorb the visible light. This demonstrates the potential of the photocatalyst to harness solar energy for degradation of dyes in water.

In view of improving TiO_2 photo efficiency under visible light, different strategies have been developed including surface plasmon sensitization. Therefore, the preparation of the visible light active photocatalysts was very crucial. In this project, gold nanoparticles (spherical and rod-shaped) were chosen to provide plasmonic properties in TiO_2 photocatalyst.

Gold nanoparticles were first synthesized on their own using the well-known seed-mediated and Turkevich methods. The colloidal nanoparticles were characterized using UV-Vis spectrophotometer and Transmission electron microscopy (TEM). The particle sizes were measure using image j software.

For the synthesis of Au/TiO_2 composites, a nucleation and growth method was adopted. TiO_2 was coated on the surface of the already prepared gold nanoparticles at 95°C for 5 hrs. UV-Vis spectrophotometer, TEM, and XRD were used to characterize the collected powder samples.

Additionally, the obtained Au/TiO_2 samples were then used for degrading model azo dyes.

ACKNOWLEDGEMENTS

The authors would like to thank the Reference Group of WRC Project **K5/2775** for their guidance and advice during the course of the project:

Name	**Institution**
Dr John Zvimba	Water Research Commission
Dr Langelihle Nsikayezwe Dlamini	University of Johannesburg
Dr Lucky Sikhwivhilu	Mintek
Mrs Ansie Smith	City of Cape Town

TABLE OF CONTENTS

EXECUTIVE SUMMARY iii

ACKNOWLEDGEMENTS iv

TABLE OF CONTENTS v

LIST OF ABBREVIATIONS vii

LIST OF FIGURES viii

LIST OF TABLES viii

CHAPTER 1 INTRODUCTION AND BACKGROUND 1

1.1. Background 1

1.2. Surface plasmon Resonance 2

1.3. Plasmon enhance mechanisms 3

CHAPTER 2 LITERATURE REVIEW 8

2.1 INTRODUCTION 8

2.2 Wastewater treatment in textile Industries 9

2.2.1 Advanced oxidation processes (AOP) 10

2.3. Semiconductors Materials for Water Treatment 13

CHAPTER 3 SYNTHESIS AND CHARACTERIZATION OF THE PHOTOCATALYSTS 15

3.1. Introduction 15

3.1.1. Synthesis of gold nanospheres 15

3.1.2. Synthesis of gold nanorods 15

3.1.3. Synthesis of Au/TiO_2 nanocomposites 15

3.2. Characterization of Au/TiO_2 photocatalysts 16

3.3. Conclusion 19

CHAPTER 4 PHOTOCATALYTIC DEGRADATION OF THE MODEL TETILE DYES USING PLASMON BASED AU/TIO_2 COMPOSITES 20

4.1. Introduction 20

4.2. Photocatalysis experiments 20

4.3. Determination of electric energy per order 20

4.4. Photocatalytic degradation of model dyes 21

4.5. Photocatalysis under direct sunlight 27

4.6. Photocatalyst Regeneration 28

4.7. Conclusion 29

CHAPTER 5 CONCLUSIONS AND RECOMMENDATIONS 30

Recommendations 30

REFERENCES 31

LIST OF ABBREVIATIONS

AuNPs	GOLD NANOPARTICLES
AuNRs	GOLD NANORODS
AuNS	GOLD NANOSPHERES
CR	CONGO RED
CTAB	HEXADECYLTRIMETHYLAMMONIM BROMIDE
FTIR	FOURIER-TRANSFORM INFRARED SPECTROSCOPY
RO16	REACTIVE ORANGE 16
SEM	SCANNING ELECTRON MICROSCOPY
SPR	SURFACE PLASMON RESONANCE
TEM	TRANSMISSION ELECTRON MICROSCOPY
UV	ULTRA-VIOLET
XRD	X-RAY CRYSTALLOGRAPHY

LIST OF FIGURES

Figure 1.1: Representation of the mechanism of plasmon enhanced photocatalysis 4
Figure 2.1: Advanced Oxidation Processes.....11
Figure 2.2: Semiconductors and their band gap (eV) energy against standard hydrogen potential (SHE).....13
Figure 3.1: UV-Visible spectra of AuNS (nanospheres) and AuNR (nanorods).....16
Figure 3.2: UV-Visible spectra of the TiO_2 and composite photocatalysts composed of AuNS (nanospheres) and AuNRs (nanorods) (AuNS/TiO_2 and AuNRs/TiO_2).....17
Figure 3.3: XRD patterns of (a) TiO_2, (b) AuNS/TiO_2 and (c) AuNRs/TiO_2. 18
Figure 3.4: TEM images of (A) AuNS, (B) AuNRs, (C) AuNS/TiO_2 and (D) AuNRs/TiO_2.....19
Figure 4.1: UV-Visible spectra for degradation of CR using (A) (AuNRs/TiO_2) and (B) (AuNS/TiO_2).....22
Figure 4.2: UV-Visible spectra for degradation of CR using (A) (AuNRs/TiO_2) and (B) (AuNS/TiO_2) 23
Figure 4.3: Pseudo-first order kinetic fits for the degradation of CR and RO 16, (A) catalyzed by AuNS/TiO_2 nanocomposites and (B) catalyzed by AuNRs/TiO_2 24
Figure 4.4: Degradation efficiency for and as a function of time using (A) RO 16 and (B) CR usingAuNS/TiO_2,AuNRs/TiO_2andTiO_2).....26
Figure 4.5: Change in concentration and degradation efficiency graphs for the degradation of (A) CR and (B) RO 16. (C) Pseudo-first order kinetic fits for the degradation CR 16 and RO 16. 28
Figure 4.6: Cyclic photocatalytic degradation of azo dyes using Au/TiO_2 photocatalyst.....29

LIST OF TABLES

Table 1.1: Plasmon enhanced photocatalytic treatment of organic pollutants 4
Table 2.1: Characteristics of process waste streams of the Textile industry (Oke, 2018)..... 9
Table 4.1: Photodegradation and kinetic properties of CR and RO16 using the Au/TiO_2 composites.....27

CHAPTER 1

INTRODUCTION AND BACKGROUND

1.1. Background

The water issues in the near foreseeable future require the development of more effective methods to remove pollutants in water. Large amounts of non-biodegradable dye pollutants are released into aquatic ecosystems. These dyes exert threats to the environment and humankind due to their carcinogenic nature. In this regard, there is a need for the development of sustainable, low-cost technologies for effective removal of dyes from textile effluents. Some of the major limitations associated with wastewater treatment technologies are: (1) the high production of sludge, a challenge in the coagulation process, and (2) the chemically stable dye structures, which make it difficult for degradation by biological processes. Organic dyes have been identified as the most persistent pollutants in textile dye effluents and azo dyes account as the major used in textile processing (Singh and Arora, 2011). Azo dyes are aromatic compounds with one or more -N=N- groups in their chemical structures (Bafana, Devi and Chakrabarti, 2011). These compounds are generally chemically stable, hence, making it difficult to degrade by conventional biological processes. Biodegradation of azo dyes results in production of carcinogenic colourless aromatic amines (McMullan *et al.*, 2001). The resulting toxic amines pose a threat on both human health and the environment. Furthermore, dyes in water reduce sunlight penetration, thereby affecting the visibility of water.

Therefore, advanced oxidation processes (AOPs) have attracted a great deal of interest due to the potential of mineralization of the organic contaminants. AOPs involve generation of hydroxyl radicals that destroy organic compounds. Among these AOPs, solar photocatalysis is a promising energy saving emerging treatment technology due to its ability to degrade organic compounds to complete mineralization at very low energy (Atul et al., 2013; Tanveer & Tezcanli Guyer, 2013). Generally, a semiconducting material is irradiated by a light source with energy higher than its band gap (E_g) to generate highly reactive oxidative species that are able to degrade the organic pollutants. The immense interest in photocatalysis is also due to the possibility of exploring solar energy for water treatment (Raji and Palanivelu, 2011). Solar energy represents the most abundant source of renewable and safe energy. For this reason, a lot of effort has been dedicated to finding semiconducting materials, which can absorb the solar spectrum.

Solar-driven photocatalytic degradation of organic pollutants in wastewater is a promising method due to the benefit of using solar energy. Metal oxide semiconductors are promising as photocatalysts for photocatalysis, however, one of their major limitations is wide band gaps. For example, a TiO_2 photocatalyst is limited to, and can only be excited by, UV light activity due to its wide band gap of 3.2 eV. To promote photocatalytic wastewater decontamination into real life applications, it is desirable to develop more reliable photocatalysts that are affordable and reusable. The great prospects for plasmon-enhanced reactions in this field have demonstrated great potential toward solar energy conversion. Solar photocatalysis has the potential to utilize

the most abundant energy to overcome the pressing issues related to water. Photocatalytic activity of metal oxides can be improved by loading surface plasmon metals into the semiconductor. Surface plasmon metals such as gold (Au) can act as photosensitizers for the photoexcitation of metal oxides under visible light, leading to visible photocatalytic activity due to the localized surface plasmon resonance (LSPR). Utilizing cheap solar energy to drive photocatalytic reactors is an ideal goal for the efficient degradation of organic pollutants in water. Plasmonic gold nanoparticles exhibit high absorption cross-sections, which facilitate the generation of hot electrons. It is, therefore, crucial to gain an in-depth understanding of the photonic processes involved increasing photocatalytic efficiency under visible light.

Aim

The development of sustainable methods of treating organic pollutants from wastewater is a desired task. However, the main problem to the realization of solar photocatalytic wastewater treatment is the limited absorption in the visible spectrum. In light of these challenges, the aim of this project was to develop visible light active photocatalysts through combination of surface plasmon metals and metal oxides. The following are the objectives of this project:

OBJECTIVE 1

Synthesis and Characterization of photocatalysts

OBJECTIVE 2

Photocatalytic degradation of organic dyes under visible light

OBJECTIVE 3

Evaluation photocatalyst re-usability.

1.2. Surface plasmon Resonance

Plasmonic nanoparticles have attracted a lot of attention due to their ability to interact with light in the visible to near infra-red (IR) spectrum (Xiao *et al.*, 2013; Zhou *et al.*, 2015). When plasmon metal nanoparticles interacts with electromagnetic radiation it triggers a collective oscillation of electrons, this phenomenon is referred to as the localized surface plasmon resonance (LSPR) (Hou and Cronin, 2013). Tuning the size, shape, surrounding dielectric medium, and distance between neighbouring objects, can manoeuvre the surface plasmon resonant wavelength. The extinction spectrum of a metal sphere with a particle size smaller than the wavelength of light can be calculated using Mie theory as follows (Willets and Van Duyne, 2007):

$$\mathrm{E}(\lambda) = \frac{24\pi^2 \mathrm{N a}^3 \varepsilon_{\mathrm{out}}^{3/2}}{\lambda \ln(10)} \left[\frac{\varepsilon_{\mathrm{i}}(\lambda)}{(\varepsilon_{\mathrm{r}}(\lambda) + \chi\varepsilon_{\mathrm{out}})^2 + \varepsilon_{\mathrm{i}}(\lambda)^2} \right] \qquad \textbf{(1.1)}$$

where $E(\lambda)$ is the extinction at a specific wavelength, ε_T and ε_i are respectively, the real and

imaginary components of the dielectric function of the metal. *N* is the number of atoms in the particle and *a* is the radius of the particle. The two components of the dielectric constant are dependent on the wavelength. The changes in the local dielectric environment can cause a shift in plasmon frequency of metal nanoparticles. However, the shape of the particles significantly affects the LSPR properties of gold nanoparticles.

In comparison with spherical AuNPs, AuNRs exhibit anisotropic optical behaviour that are governed by their dimensions (Akouibaa, Benhamou and Derouiche, 2013). As a result, AuNRs have two plasmon modes, the longitudinal mode and the transverse mode. Gold nanorods offer advantages in this respect since the longitudinal mode can be tuned across the visible to near infrared regions of the spectrum, thus covering a broad spectral range. For gold nanorods, the LSPR can be predicted by Gans theory (Akouibaa, Benhamou and Derouiche, 2013), where the extinction cross-section is given by:

$$C_{ext} = \frac{2\pi V}{3\lambda}\,\varepsilon_m^{3/2}\sum_j \frac{\left(\frac{1}{P_j^2}\right)\varepsilon_2}{\left(\varepsilon_1 + \frac{1-P_j}{P_j}\,\varepsilon_m\right)^2 + \varepsilon_2^2} \qquad \textbf{(1.2)}$$

Where V is the volume of the rod, ε is the dielectric constant of the surrounding medium and P_j is the depolarization factor. For the elongated particles the depolarization factor is given by:

$$P_{length} = \frac{1-e^2}{e^2}\left[\frac{1}{2}\ln\left(\frac{1+e}{1-e}\right) - 1\right] \qquad \textbf{(1.3)}$$

$$P_{width} = \frac{1 - P_{length}}{2} \qquad \textbf{(1.4)}$$

$$e^2 = 1 - (\text{aspect ratio})^{-2} \qquad \textbf{(1.5)}$$

Gold nanorods exhibit two distinct plasmon peaks (a longitudinal peak and a transverse peak. Varying the aspect ratio(length/width) of the gold nanorods allows for tuning of the longitudinal peak from the visible to the near infrared.

1.3. Plasmon enhance mechanisms

The combination of wide band gap photocatalysts with noble metals significantly enhances their photoactivity under the visible light. For example, TiO_2 being a wide band photocatalyst can be tuned to absorb in the visible to IR region of the solar spectrum. In plasmon-enhanced photocatalysis there are two main enhancement mechanisms known as hot electron injection mechanism and near field enhancement mechanism.

In a hot electron injection mechanism, the surface plasmon of the metal nanoparticles can be excited with visible light and the hot electrons are transferred into the conduction band of the semiconductor (Zhou *et al.*, 2015; Mondal and Sharma, 2016). The holes (h^+) generated in the plasmonic metal react with the water molecules on the surface and generate the hydroxyl radicals (·OH). These hydroxyl radicals are responsible for the degradation of the organic pollutants. On the other hand**,** the electrons in the conduction band of the semiconductor react with oxygen to generate reactive superoxide radicals($\cdot O_2^-$). The mechanism of charge injection from metal to TiO_2 is applicable when the metal NPs and TiO_2 are in close contact with each other, allowing for the facile electron transfer.

The second mechanism is called the near field enhancement, where the SPR electrons interact with the electromagnetic field surrounding it, which results in enhancement in the intensity of the surrounding electric field (hot spots) (Khan *et al.*, 2015). The generation of the charge carriers is directly proportional to the intensity of the local electric field. In addition, the presence of the plasmon metals prevents electron/hole recombination, which improves the photocatalysis efficiency. The mechanisms discussed above are illustrated in **Figure 1.1**. Through such plasmon enhanced mechanisms, plasmonic metals are able to photosensitize the wide-band-gap semiconductors such as TiO_2, hence, extending their absorption range.

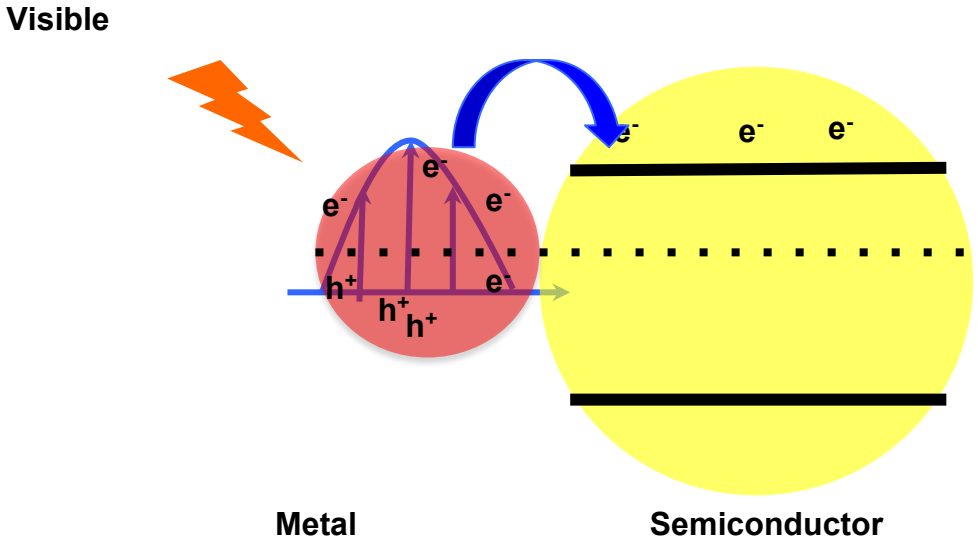

Figure 1.1: Representation of the mechanism of plasmon enhanced photocatalysis.

Various pollutants have been degraded using plasmon-enhanced mechanism under visible light and these are summarized in **Table 1.1.** Copper (I) oxide (Cu_2O) nanostructures decorated with plasmon copper (Cu) nanoparticles showed an enhanced photocatalytic activity of about 88% in 60 mins compared to 52% when Cu_2O was used alone (Cheng *et al.*, 2016). This study shows that the presence of plasmon nanoparticles played an important role of enhancing the photocatalytic activity. When silver nanoparticles were incorporated into ZnO about 82%

degradation efficiency was achieved under visible light. However, pure ZnO nanoparticles did not show any significant activity (Liu, Wei and Gao, 2015). This effect was attributed to the photo-induced charge generation and the formation of a Schottky barrier between the Ag nanoparticles and the semiconductor ZnO, which then allowed the transfer of the excited electrons from the metal into the conduction band of the semiconductor. In another study, gold nanoparticles@ZnO core-shell nanoparticles were used to degrade rhodamine blue, methyl orange and methyl blue using simulated sunlight light. The study shows that the incorporation of the plasmon nanoparticles enabled visible photocatalysis in a UV absorbing semiconductor (Sun *et al.*, 2016). The degradation of methylene blue using Au/TiO_2 was also reported by (Chen *et al.*, 2015). It was observed that the photocatalytic activity increased with the amount of gold nanoparticles, which shows a clear effect of the activity on the plasmon gold nanoparticle.

Plasmon nanometals represent a class of promising materials for application in solar photocatalysis because of their strong ability to interact with visible light. These structures exhibit higher absorption cross-sections, which makes them more desirable for solar energy conversion. In this project, the surface plasmon of the gold nanosphere and nanorods was explored for the plasmonic sensitization of the TiO_2.

Table 1.1: Plasmon enhanced photocatalytic treatment of organic pollutants.

Catalyst	Pollutant	Light source	Degradation Efficiency	Time	Method of synthesis	Crystalline phase	Ref.
Au/TiO_2	Methylene Blue	300 W Xe-lamp, Microsolar 300 UV, Ultra-violet (UV)/Visible	UV (66%) Visible (49%)	120 min	Hydrothermal and microwave	nanosheet	(Chen *et al.*, 2015)
Ag/ZnO	RhB	9 W blue light lamp, Visible	82%	240 min	Photoreduction	Rods	(Liu, Wei and Gao, 2015)
Cu_2O-Cu	Methylene Blue	90 W tungsten lamp, Visible	52%	60 min	Redox procedure	Microspheres	(Cheng *et al.*, 2016)
Pt/TiO_2	Phenol, 2-chlorophenol	450 W mercury lamp UV	Phenol (87.7%), (100%)	120 min	Colloidal routes	Rutile	(Barakat *et al.*, 2014)
Au/Ag/TiO_2	Methylene Blue	633 nm helium-neon laser, visible	86%	180 min	Facile chemical	nanorods	(Zhou *et al.*, 2013)
Au/ZnO	(RhB)	300 W Xenon lamp, visible	84.5%	180 min	Polyol	octahedral	(Sun *et al.*, 2016)
Ag@AgCl/Cu_2O	Methylene Blue	250 W Xenon lamp, visible	93.6%	120 min	Precipitation in situ photoreduction	Octahedral	(Liu *et al.*, 2015)
Au/Cu_2O	Methyl orange	500 W Xenon lamp, visible	86%	80 min	Facile solution route	Cuboctahedron	(Wang *et al.*, 2016)

Catalyst	Pollutant	Light source	Degradation Efficiency	Time	Method of synthesis	Crystalline phase	Ref.
Au/Cu_2O	Methyl orange	500 W Xenon lamp, visible	94%	80 min	Facile solution route	Octahedral	(Yuan *et al.*, 2015)
CuO/Ag/AgCl/TiO_2	Methyl orange, phenol	Xe lamp (AULLT Cell-HFX300), Visible	91% (MO) 71 (phenol)	25 min 50 min	Reverse microemulsion	Anatase, rutile	(Shah *et al.*, 2015)

CHAPTER 2
LITERATURE REVIEW

2.1 INTRODUCTION

In South Africa, the textile industries are concentrated in the Western Cape, KwaZulu-Natal, the Free State and Gauteng provinces (Vlok, 2006). The textile industry is the sixth largest employer in the manufacturing sector and eleventh largest exporter of manufactured goods in South Africa (Gravelet-Blondin *et al.*, 1997). This industry accounts for about 15% of total formal employment which, however, has since declined dramatically over the last few years. Textile exports in South Africa have also declined by 35.6% between years 2003 and 2004 due to the imports from china and lack of investments (Vlok, 2006).

Large quantities of water are used in textile operations, and as a result, huge quantities of wastewater are generated from these processes. Averagely, 50-150 L of water is required for processing 1kg of textile material depending on the type of process (Samanta *et al.*, 2019). Textile industries apply various kinds of synthetic dyes, and hence, have to deal with large volumes of highly coloured wastewater. This industry is currently facing problems with respect to environmental legislation due to issues concerning the toxicity of the effluents, colour and high chemical oxygen demand (COD) (Gravelet-Blondin *et al.*, 1997).

Textile industries are classified according to the nature of fabrics they produce, including: (1) protein fabrics, which come from animals (e.g. wool, silk and mohair), (2) cellulosic materials obtained from plants (e.g. cotton, rayon and linen), and (3) artificially produced fabrics (e.g. nylon, polyester and acrylic) (Ananthashankar, 2014; Holkar *et al.*, 2016). The type of dyes used in the textile industry depends on the fabrics they produce. For example, cellulose fibres are dyed using reactive dyes, direct dyes, naphthol dyes and indigo dyes. Acid dyes are used for dyeing protein fibres, and reactive dyes and azo dyes for dyeing cotton fibers. Textile dyes may be classified according to chemical structure or application (Benkhaya et al., 2017). Textile processing technology consists of desizing, scouring, bleaching, mercerizing, dyeing, printing and finishing processes (Access, 2018). The wet processes consume large volume of water and release highly coloured effluents. Textile wastewater is also found to contain toxic metals and solids (Oke, 2018). The characteristic effluents and the possible contaminants from each textile-processing step is described in **Table 2.1**. During the dyeing stage, various dyes are used to add colour to the fibres, and water is used to transfer dyes into a solution form. These dyes end up in textile industry effluents and are the cause of highly coloured wastewater

Table 2.1: Characteristics of process waste streams of the Textile industry (Oke, 2018).

Process	Possible Pollutants	Nature of Wastewater
Desizing	Starch, glucose, enzymes, waxes, PVA.	BOD 35-50%
Scouring	Grease, soda ash, sodium phosphate, fibers, surfactants, waxes, caustic soda.	Dark coloured, dissolved solids, BOD 30%
Bleaching	NaOH, Na_2O_2, H_2O_2, Cl_2	Alkaline, BOD 5%
Mercerizing	Na_2CO_3, H_2SO_4, NaOH	Strongly alkaline, BOD> 1%
Dyeing	Dyes, detergents, metal salts, urea	Strong colour, heavy metals, BOD 5%
Printing	Acids, Oils, pigments, gums, cross-linkers	Oily, strong colour, BOD 6-10%
Finishing	Hydrocarbon, resins, waxes, formaldehyde, softeners	Slightly alkaline, Low BOD (2-4%)

2.2 Wastewater treatment in textile Industries

The wastewater produced from the textile industry requires to be cleaned from colour and chemicals, which are used during the production processes. Thus, before discharge of textile effluents, they are treated using treatment processes, such as physical, chemical and biological treatment processes. The traditional methods for treating textile wastewater include coagulation/flocculation, electrocoagulation, and adsorption, biological and reverse membrane Filtration (Sen, 2015). These processes have their own advantages and disadvantages. Coagulation-flocculation methods are used to eliminate mainly disperse and sulphur dyes, however, demonstrate very low removal efficacy for reactive and acid dyes (Designing, 2016). Adsorption technology is capable of adsorbing various dyes in solution, but this technique generates a lot of sludge (Shireesha *et al.*, 2017). Filtration technologies which include microfiltration, ultrafiltration, nanofiltration, and reverse osmosis are able to remove all types of dyes. However, the disadvantages include the high cost of membranes and high working pressure required to push the wastewater flow through membrane. Advanced oxidation processes (AOPs) have been widely considered to remove the non-biodegradable organic dyes.

2.2.1 Advanced oxidation processes (AOP)

AOPs have received substantial attention over the years owing to their ability to degrade organic compounds to CO_2 and H_2O and no sludge production. They are characterized by the production of the ·OH radical, which has high oxidation potential (Goi, 2005). The hydroxyl radical is a non-selective oxidizing species, which can react with organic compounds by electrophilic addition of OH^- group (**Reaction 2.1**) or by abstracting a hydrogen atom (**Reaction 2.1 and 2.2**) (Stasinakis, 2008).

$$OH^{\cdot} + R \rightarrow ROH \quad \textbf{(2.1)}$$

$$OH^{\cdot} + RH \rightarrow R^{\cdot} + H_2O \quad \textbf{(2.2)}$$

AOPs include a group of processes (**Figure 2.1**) such as photocatalysis, sonolysis, radiation, electrochemical oxidation, Fenton and ozone. AOPs are used for the degradation of non-biodegradable organic compounds, which cannot be removed by biological methods. These processes can be enhanced by careful optimization of several parameters, including contact time, reagent dosage, irradiation energy, and as well as reactor configuration. AOPs may be used as pre-treatment step (where they convert non-biodegradable organic compounds to more degradable) or post treatment in combination other treatment technologies (Nidheesh, Zhou and Oturan, 2018). The major disadvantage for the use of AOPs as a pre-treatment step is the high dosage of the reagents. Various AOPs have been used to degrade persistent organic compounds that are present in textile wastewater in combination with biological processes.

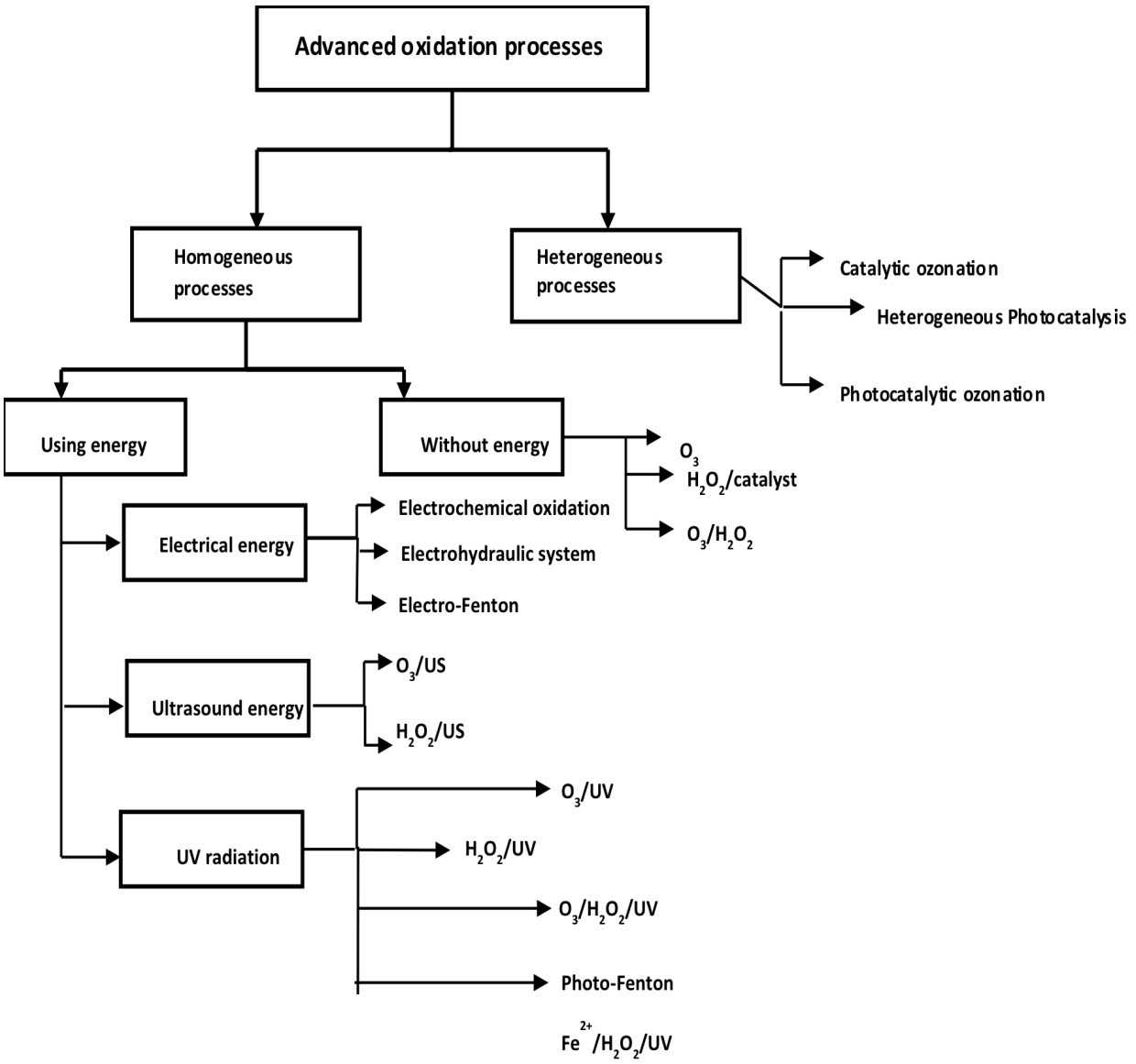

Figure 2.1: Advanced Oxidation Processes.

(i) Fenton oxidation process

Among AOPs, the Fenton process is the most used owing to its advantages such as rapid degradation of the range of organics and simple operation (Rahim Pouran, Abdul Aziz and Wan Daud, 2015). Fenton oxidation process involves a rapid reaction between hydrogen peroxide and iron and a subsequent production of hydroxyl radicals. In the first step of the Fenton process ferrous ions are oxidized to ferric ions in acidic media, according to **equation 2.3** and **2.4**.

$$Fe^{2+} + H_2O_2 \rightarrow Fe^{3+} + OH^{\cdot} + OH^{-} \quad \textbf{(2.3)}$$

The ferric ions are then reduced back to ferrous.

$$Fe^{3+} + H_2O_2 \rightarrow Fe^{2+} + HO_2^{\cdot} + H^{+} \quad \textbf{(2.4)}$$

A number of factors influence the efficiency of the fenton oxidation process such as, pH, temperature and hydrogen peroxide. This process gained its popularity because it does not require any energy input to activate the hydrogen peroxide. However, the main drawback of this process relates to the handling and storage of the hydrogen peroxide. Therefore, this has led to the development of the photo-fenton oxidative process, which use UV light to reduce the ferric ions back to ferrous ions as in **equations 2.5** and **2.6**.

$$Fe^{3+} + hv \rightarrow Fe^{2+} + OH^{\cdot} \quad \textbf{(2.5)}$$

$$H_2O_2 + hv \rightarrow 2\,OH^{\cdot} \quad \textbf{(2.6)}$$

UV light irradiation increases the rate of the reaction due to an increased production of hydroxyl radicals. However, UV irradiation increases the cost of the process. Therefore, processes that use solar energy are more appealing for sustainability.

(ii) Photocatalysis

Photocatalysis has appeared as a promising method degradation of organic pollutants using sunlight. Photocatalysis takes place when the semiconductor is irradiated by energy equal or greater than its band gap, the valence electron (**e**$^-$) is then excited to the conduction band leaving behind a hole (**h**$^+$) in the valence band.

$$\text{Photocatalyst} + hv \rightarrow e^-_{(CB)} + h^+_{(VB)} \quad \textbf{(2.7)}$$

The photogenerated electron reacts with molecular oxygen to form a superoxide radical O_2.

$$O_2 + e^- \rightarrow + h^+_{(VB)} \quad \textbf{(2.8)}$$

$$O_2 + e^- \rightarrow O_2^{\cdot} \quad \textbf{(2.9)}$$

The photogenerated holes react with water to produce OH^- radical.

$$h^+ + H_2O \rightarrow OH^{\cdot} + h^+ \quad \textbf{(2.10)}$$

$$h^+ + OH^- \rightarrow OH^{\cdot} \quad \textbf{(2.11)}$$

The superoxide ($\mathbf{O_2^-}$) produced gets protonated forming hydroperoxyl radical ($\mathbf{HO_2^-}$) and then subsequently $\mathbf{OH^-}$**,** which further dissociates into highly reactive hydroxyl radicals (**·OH**).

$$O_2^{\cdot -} + h^+ \rightarrow HOO^- \quad \textbf{(2.12)}$$

$$e^- + HOO^- \rightarrow HO_2^- \quad \textbf{(2.13)}$$

$$2\,HOO^{\cdot} \rightarrow H_2O_2 + O_2 \quad \textbf{(2.14)}$$

$$H_2O_2 \rightarrow +2OH^{\cdot} \quad \textbf{(2.15)}$$

The hydroxyl radical (·OH**)** is the main oxidizing agent; it aids the degradation of organic pollutants into carbon dioxide and water. This radical has a higher oxidizing power (2.80 V) compared to other common oxidants such as O_3 (2.07 V), H_2O_2 (1.77 V) and chlorine (1.36 V) (Pelaez *et al.*, 2012). The superoxide anion (O_2^{-}) and the hydrogen peroxide radical (H_2O_2) also participate in the mineralization of organic molecules. The overall mechanism for the oxidation of organic pollutants can be denoted using **equation 2.16**:

$$OH^{-} + \text{organic pollutant} \rightarrow CO_2 + H_2O \quad \textbf{(2.16)}$$

2.3. Semiconductors Materials for Water Treatment

Metal oxide semiconductors have received considerable interest in photocatalytic treatment of organic pollutants because of their ability to absorb light energy and produce charge carriers. Various semiconductor materials have been studied such as TiO_2 (Vinu, Akki and Madras, 2010; Pattanaik and Sahoo, 2013), and ZnO (Baruah, Pal and Dutta, 2012). For the photocatalytic degradation of the organic compounds to happen, the valence band of the photocatalyst should lie at a more positive potential than the oxidation potential of the hydroxyl radicals (E^0 ($H_2O/OH^{\bullet}$) = 2.8 V vs NHE) and the conduction band must be positioned at a more negative potential than the reduction potential of the oxygen radicals (E^0 ($O_2/O_2^{\bullet -}$) = −0.28 V vs NHE). Titanium dioxides (TiO_2), zinc oxide (ZnO), zirconium dioxide (ZrO_2), tungsten oxide (WO_2) are the typical photocatalyst materials for water treatment**. Figure 2.2** (Wu, Changzhong Jiang and Roy, 2014) illustrates the band position for the different semiconductors along with their respective redox potentials.

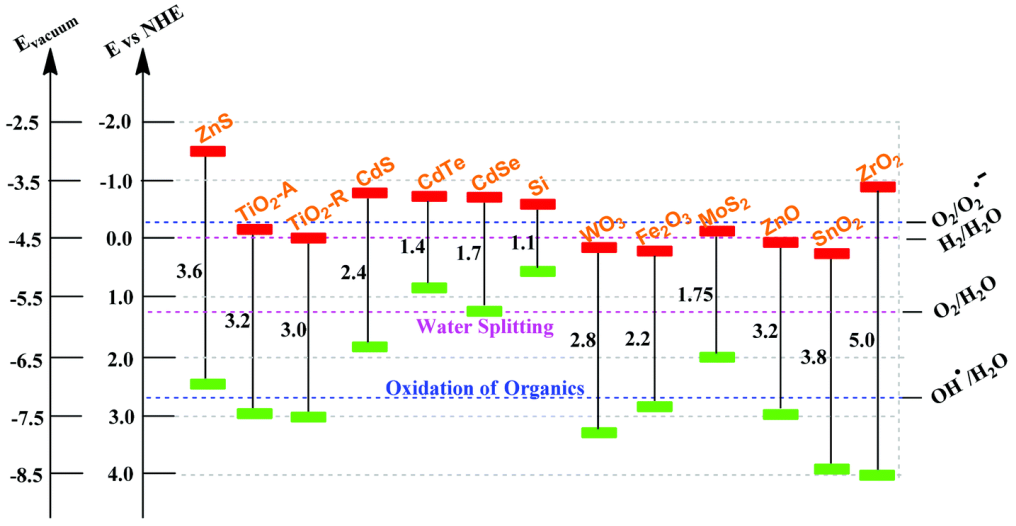

Figure 2.2: Semiconductors and their band gap (eV) energy against standard hydrogen potential (SHE) (Wang et al., 2017).

Titanium dioxide (TiO_2) exists in nature in three crystal phases: anatase (tetragonal), rutile (tetragonal), and brookite (orthorhombic) (Munirah *et al.*, 2018). TiO_2 is an n-type semiconductor with a band gap of 3.0 and 3.2 eV for rutile and anatase respectively (Lan, Lu and Ren, 2013). The rutile phase is the more thermodynamically stable of all the phases. The brookite phase is rare and is very thermodynamically unstable, and thus it is the least studied. Brookite is an indirect band gap semiconductor and, therefore, it is not photoactive. TiO_2 is non-toxic, low cost, and resistant to photocorrosion, and thus the most investigated photocatalyst. TiO_2 semiconductor photocatalyst, can be prepared by a sol-gel, and/or hydrothermal/solvothermal method (Gupta and Tripathi, 2012). The photocatalytic performance of metal oxides photocatalysts is influenced by their physicochemical properties, for example crystallinity, morphology and surface properties. It has been demonstrated that the type of the facet exposed influences the photocatalytic performance (Liu *et al.*, 2011). In TiO_2, the {001} facets showed higher photocatalytic activity compared to the {101} facets on the photodegradation of methylene blue (Liu et al., 2010; D'Arienzo et al., 2011; Ma et al., 2010). A higher photocatalytic activity of the {001} facet in anatase-TiO_2 for the degradation of methyl orange was also reported by Han et al. (2009). The {101} facets participate in the reduction processes, while {001} facets are involved in the oxidative processes (Ohno, Sarukawa and Matsumura, 2002; Ye *et al.*, 2013).

TiO_2 is, so for, the most wildly used photocatalyst due to its advantages such as high stability, non-toxicity and most abundant. However, one of the major disadvantages of TiO_2 is its wide bandgap, which means it only absorbs ultraviolet light. Combination of surface plasmon nanoparticles such as Au with TiO_2 is of great importance for the rational design of hybrid materials for solar energy utilization in wastewater treatment. Therefore, the purpose of this study was to improve the photocatalytic activity of TiO_2 under visible irradiation by incorporating gold plasmon nanoparticles for the treatment of textile azo dyes.

CHAPTER 3

SYNTHESIS AND CHARACTERIZATION OF THE PHOTOCATALYSTS

3.1. Introduction

This chapter deals with the synthesis and characterization of the photocatalysts used in this study. The experimental protocols for the synthesis of AuNS, AuNRs and Au/TiO_2 composite photocatalysts are also detailed. Lastly, the results of the characterisation of the AuNS, AuNRs and Au/TiO2 photocatalysts also are discussed.

3.1.1. Synthesis of gold nanospheres

Gold NPs were prepared according to the Turkevich method through the reduction of a $HAuCl_4.3H_2O$ solution with sodium citrate (Tran *et al.*, 2016). Briefly, 36 mg of $HAuCl_4.3H_2O$ was dissolved in 200 mL of distilled water under magnetic stirring. The solution mixture was heated to boil then 10 mL of a 1% sodium citrate was added rapidly. The flask was kept refluxing for another 30 min. The deep-red colloidal solution of gold nanoparticles was then cooled to room temperature.

3.1.2. Synthesis of gold nanorods

Gold nanorods were prepared by a seed-mediated growth method (Tran *et al.*, 2016). Briefly, Au seeds are prepared by reducing 10 mL of an aqueous solution containing 0.25 mM gold tetrachloride ($HAuCl_4.3H_2O$) in 0.1 M cetyltrimethylammonium bromide (CTAB), adding 0.6 mL of 0.01 M $NaBH_4$. The solution was left to stand for 2 hrs. The growth solution was prepared by mixing 10 mL of 0.1 M CTAB, 5 mL of 1×10^{-4} M HAuCl4 and 0.004 M $AgNO_3$ (0.5 mL). To this solution, 0.07 mL of 0.1 M ascorbic acid (A.A) was added until the reaction turned colourless. Then the seed solution (15 µL) prepared above was added and the mixture hand shaken and left undisturbed at about 37°C for 24 h. The solution of gold nanorods was centrifuged at 200 rpm, the supernatant was removed and the resulting pellet of AuNRs was re-dissolved in distilled water.

3.1.3. Synthesis of Au/TiO_2 nanocomposites

AuNRs/TiO_2 composites was synthesized using nucleation and growth method (Li *et al.*, 2014) with modifications. The prepared AuNRs samples were centrifuged and dispersed in CTAB solution (8 mL, 0.025 M). The EDTA-NH_3 solution (1.4 mL) and a solution of titanium butoxide (2 mL, 2 mM) were added into the Au-NRS solution. The mixture was stirred for 30 minutes at room temperature and dried in an oven at 95°C for 5 h.

3.2. Characterization of Au/TiO_2 photocatalysts

The optical properties of gold nanoparticles are dependent on their shape and size. The UV-Vis spectrophotometer was used to study the optical properties of the gold nanoparticles before combining with TiO_2 and the Au/TiO_2 composite photocatalysts. The UV-Visible spectrum in **Figure 3.1** of the spherical gold nanoparticles shows an SPR band at 527 nm maximum. The absorption spectrum of gold nanorods shows two peaks due to anisotropy, the transversal (528 nm) and longitudinal peaks (721 nm), respectively. **Figure 3.1** shows the UV-Visible absorption of the TiO_2 nanoparticles and Au/TiO_2 nanocomposites. TiO_2 nanoparticles show an absorption peak at 351 nm, which corresponds to the band gap of 3.53 eV as calculated from **equation 3.1.**

$$E_g = \frac{1240}{\lambda} \qquad \textbf{(3.1)}$$

Where E_g (eV) is the bang gap and λ is the wavelength (nm). The SPR bands in the composites appear in the visible region, which will facilitate the absorption of the visible light by these materials. The insert picture shows the picture of TiO_2 sample and Au/TiO_2 nanocomposites, respectively, which displays a purple colour of the composite due to the presence of the gold nanoparticles.

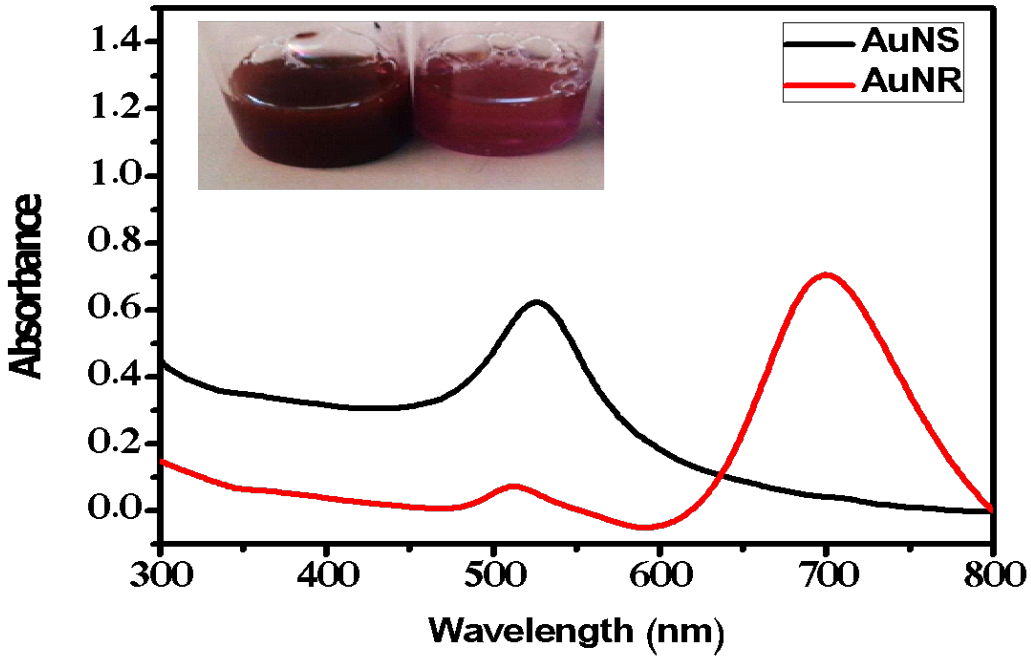

Figure 3.1: UV-Visible spectra of AuNS (nanospheres) and AuNR (nanorods).

The absorption spectra of the Au/TiO_2 composites show absorption peaks due to both the TiO_2 and the gold nanoparticles. The first peak around 351 nm is red shifted to 361 nm in the composite materials compared to the TiO_2 nanoparticles, which indicates the formation of the composite material. The barrier height between the semiconductor and the metal is of vital importance in photocatalysis. The barrier height θ_{SB} at the interface is given by **equation 3.2** since the work

function of Au is higher than the electron affinity of TiO_2 (Jiao *et al.*, 2015). The value of θ_{SB} in Au/TiO_2 is 0.8 eV.

$$\theta_{SB} = \theta_M - \chi_S \quad \textbf{(3.2)}$$

Whereθ_M, θ_{SB} and χ_S is the work function of Au, barrier height and electron affinity of TiO_2 respectively. The work function (θ_M) of Au is 5.1 eV and the electron affinity (χ_S) of TiO_2 is 4.3 eV (Jiao *et al.*, 2015). The higher the Schottky barrier height, the higher the ability of the metal to trap electrons, and preventing them from falling back to TiO_2. Au has a high work function compared to TiO_2, due to this difference in work function the electron transfer will be from TiO_2 to Au interface for the equilibration of the Fermi level, and that results in the reduction of the work function of Au/TiO_2 nanocomposites. The reduction of the work function of Au/TiO_2 means that more charge migration at the interface of the catalyst (Khoa et al., 2014).

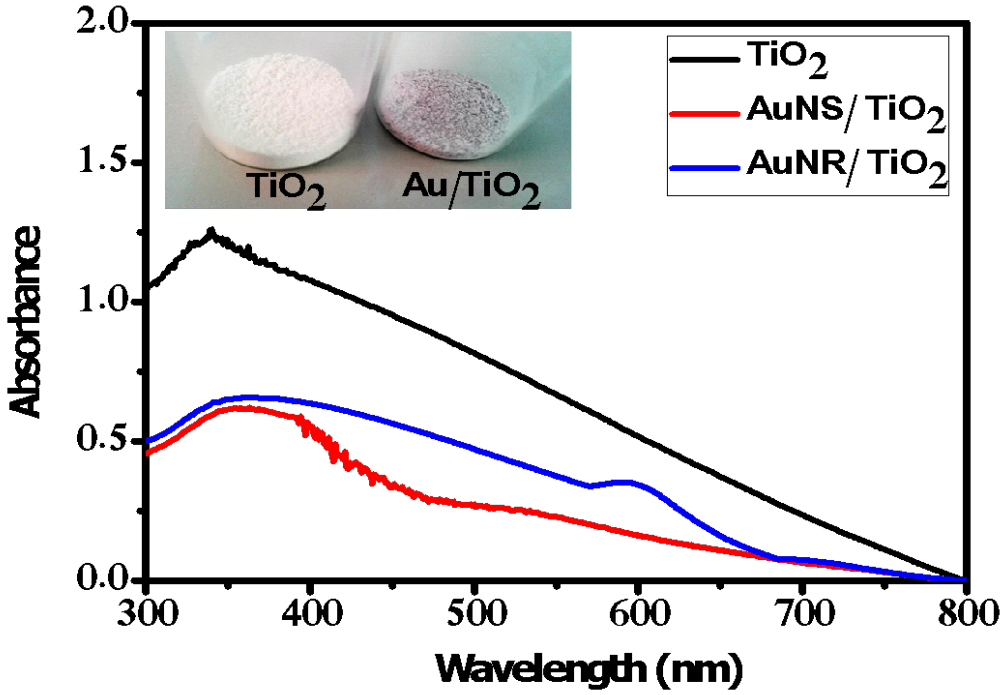

Figure 3.2: UV-Visible spectra of the TiO_2 and composite photocatalysts composed of AuNS (nanospheres) and AuNRs (nanorods) ($AuNS/TiO_2$ and $AuNRs/TiO_2$).

The XRD pattern **(Figure 3.3**) of the TiO_2 nanoparticles and the Au/TiO_2 composites exhibit peaks that corresponds to (101), (004), (200), (211), (204), (116), (220), (215), (224). The observed peaks are indexed to the crystalline anatase structure of the TiO_2. The TiO_2 in the composite maintained the same crystalline structure, however the AuNPS peaks were detected at very low levels because the gold is embedded inside the TiO_2. The small AuNPs peaks in the XRD pattern of Au/TiO_2 composites were consistent with (111), and (200).

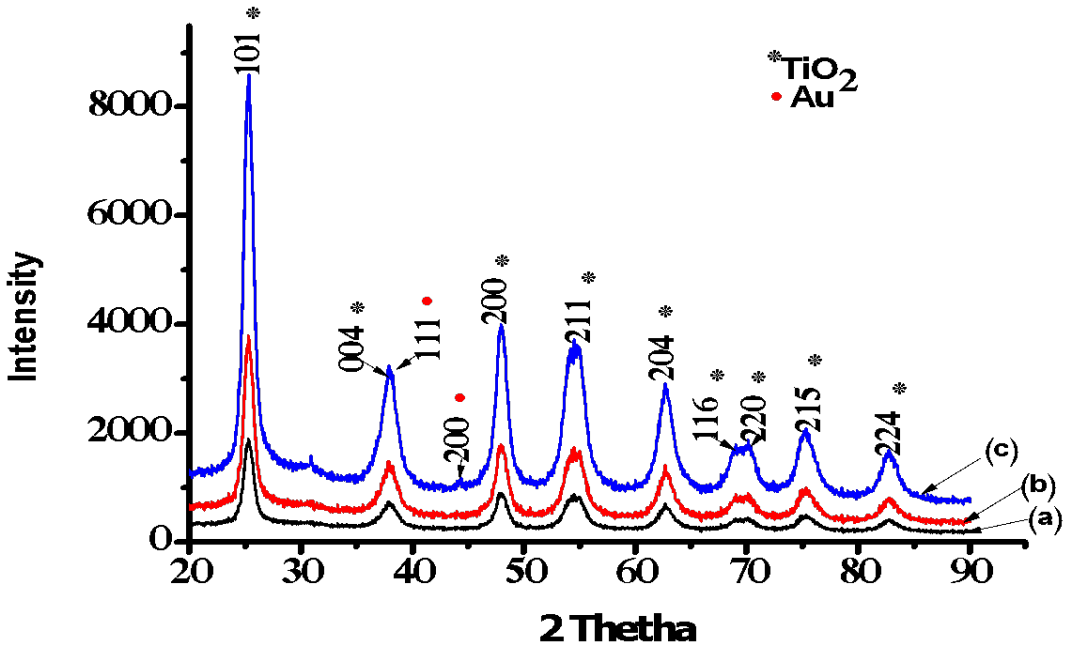

Figure 3.3: XRD patterns of (a) TiO_2, (b) AuNS/TiO_2 and (c) AuNRs/TiO_2.

HRTEM of the nanospheres, nanorods, AuNS/TiO_2 nanocomposite and AuNRs/TiO_2 nanocomposite are shown in **Figure 3.4**. The particle sizes from TEM images were measured using image J software. **Figure 3.4A** shows TEM image of gold nanospheres with an average particle size of 6.7 nm and (B) gold nanorods with an average aspect ratio (length/width) of 3.2 nm, respectively. The TEM images in **Figure 3.4C and D** show gold nanostructures embedded in TiO_2, which confirms the formation of composite nanostructures.

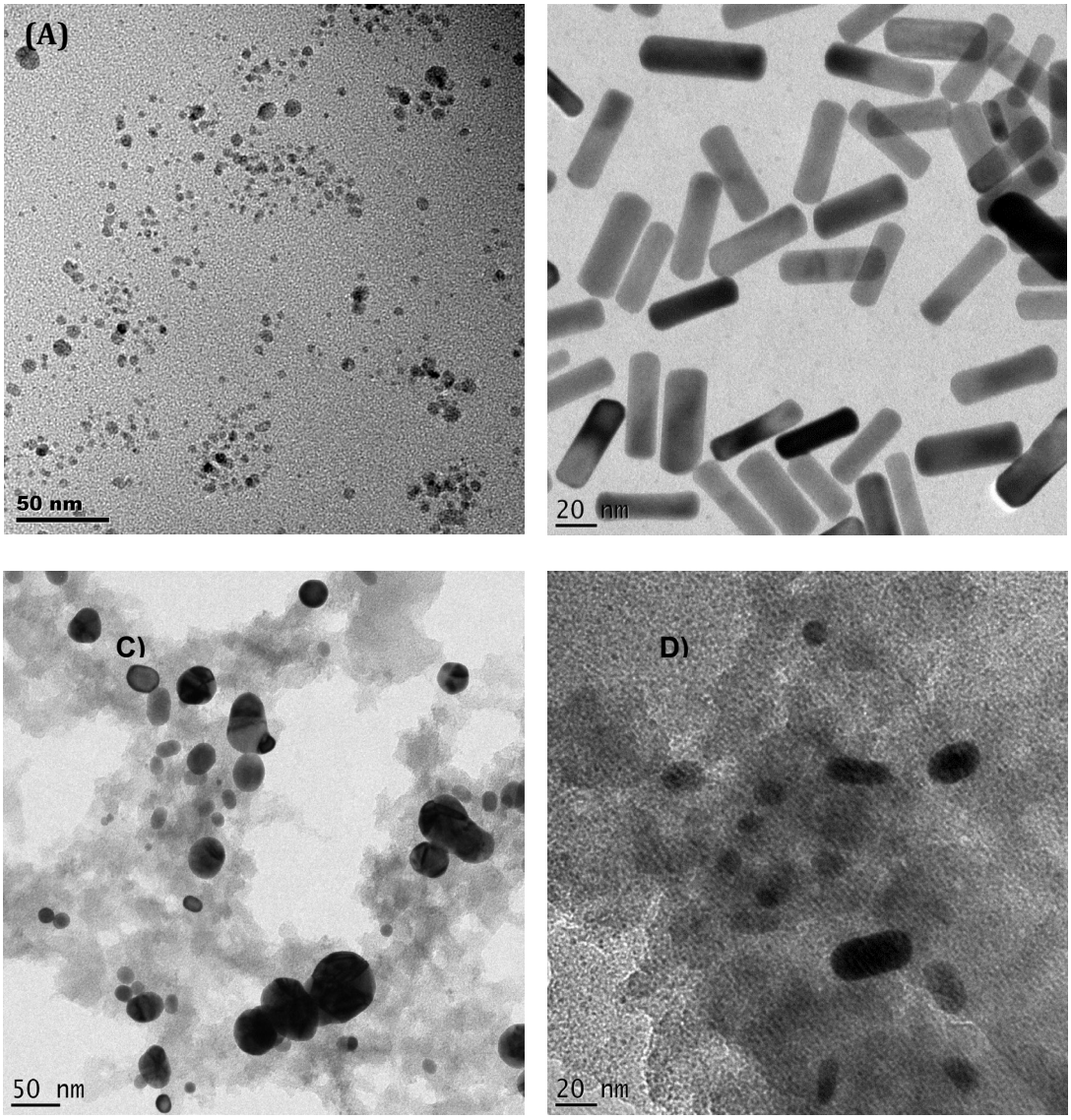

Figure 3.4: TEM images of (A) AuNS, (B) AuNRs, (C) AuNS/TiO_2 and (D) AuNRs/TiO_2.

3.3. Conclusion

In this work, Au/TiO_2 nanocomposites were synthesized by nucleation and growth method. The shape and the size of the AuNPs and the composites were defined from the TEM analysis. The TEM images also show both the gold nanoparticles and TiO_2 confirming the formation of the composite material. X-ray diffraction (XRD) results indicated that phase structures the composite samples were the of the anatase phase. UV-Vis absorption spectroscopy technique showed peaks in the visible region that were attributed to surface plasmon resonance modes of the Au NPs.

CHAPTER 4
PHOTOCATALYTIC DEGRADATION OF THE MODEL TEXTILE DYES USING PLASMON BASED AU/TiO_2 COMPOSITES

4.1. Introduction

The recent and rapid development of localized surface plasmon resonance (LSPR) photosensitization has offered a new opportunity to overcome the limited efficiency of photocatalysts. Great effort is being put into harvesting longer-wavelength visible light which accounts for a larger proportion of solar energy. Because the SPR is significantly influenced by the shape of the nanoparticles, the efficiency of plasmonic mechanisms in Au/TiO_2 photocatalysts may be tuned by altering the shape of Au NPs. Therefore, this chapter reports on the photocatalytic degradation of the model textile dyes using two different photocatalysts (AuNS/TiO_2 and AuNRs/TiO_2). The difference between the two photocatalysts is that they contain different shapes of gold nanoparticles, the nanospheres (AuNS) and nanorods (AuNRs).

4.2. Photocatalysis experiments

A 20 mg/L of the dye solution was mixed with nanoparticles (0.1 mg/mL) and stirred for 10 min in dark to achieve adsorption-desorption equilibrium. Visible light photocatalytic studies were performed with a 300 W using General Electric Quartz lamp (300 W), and a cut-off optical filter of λ>420 nm was used to filter off UV light. The reaction was conducted at 30 ± 1°C. During the irradiation of the light, about 4 ml of the solution was continuously taken at regular intervals of time. The collected samples were then centrifuged to remove any catalyst particles present in the solution for analysis by UV-Visible spectrophotometer. The removal rate of the dye can be calculated as follows:

$$\text{removal}\ (\%) = 100 \times \frac{(C_0 - C)}{C_0} \quad \textbf{(4.1)}$$

Where C_0 and C are the concentrations of the dye at t=0 and t=t, respectively.

4.3. Determination of electric energy per order

The electrical energy per order (E_{EO}), is defined as the number of kilowatt hours of electrical energy required to remove 90% of a pollutant in a unit volume of contaminated water. E_{EO} (kWh/m^3/order) can be calculated from the following equation for a batch type (Bolton *et al.*, 2001):

$$E_{Eo} = \frac{P \times t \times 1000}{V \times 60 \times \log\left(\frac{C_0}{C}\right)} \quad \textbf{(4.2)}$$

$$\ln\left(\frac{C_0}{C}\right) = k \times t \quad \textbf{(4.3)}$$

Where P is the power (kW) of the system, t (h) is the duration, V (L) is the treated volume, and C_0 and C the initial and final dye concentrations (mg/L), respectively and k is the pseudo-first order rate constant (min^{-1}).

Eqs. (5.1) and (5.2) can be written as follows:

$$\frac{34.8 \times P}{V \times k} \quad \textbf{(4.4)}$$

4.4. Photocatalytic degradation of model dyes

Deposition of gold nanoparticles on TiO_2 surface is expected to improve the photocatalytic efficiency through the plasmon mechanisms discussed in **Chapter 2**. Moreover, gold nanoparticles induce visible light photoresponse in TiO_2. The photocatalytic activity of AuNRs/TiO_2 and AuNS/TiO_2 has been evaluated for the photodegradation of reactive orange 16 and congo red as a model textile dyes under visible light irradiation**. Figure 4.1A** and **Figure 4.1B** shows the degradation of CR dye by AuNRs/TiO_2 and AuNS/TiO_2, respectively. Congo red (CR) shows a maximum absorption peak at 598 nm and reactive orange 16 (RO 16) at 490 nm and the decolourization efficiency was evaluated with respect to the change in intensity of these peaks. After 10 minutes, the 598 nm peak red shifted to 617 nm, then decreases as a function of reaction time. The red shifting of the 598 nm peaks to 617 nm is attributed to the interaction between the catalysts and the dyes. Moreover, the decolourization was accompanied by a significant decrease of the characteristic absorption peaks of the two dyes suggesting the cleavage of the azo bonds by the oxidative radicals. The graphs showing the decolourization of RO 16 dye are presented in **Figure 4.2A** and **B**. Interestingly, AuNS/TiO_2 demonstrated high adsorption of the dye molecules in the dark, which was manifested by huge decrease of the peak intensity at 490 nm. The high adsorbing property of this photocatalyst was due to the large surface area of the small spherical gold nanoparticles. However, due to the anisotropic nature of the nanorods, this behaviour was not observed for the photocatalysts containing nanorods. Both photocatalysts (AuNS/TiO_2 and AuNRs/TiO_2) demonstrated higher photodegradation of the RO 16 (monoazo dye) compared to the CR (diazo dye) due to the structural differences between the two dyes. Compared to CR which is a diazo dye, RO 16 dye contains one azo groups. The degradation and decolourization of azo dyes follows a nucleophilic cleavage of the azo bonds, hence, an increase in the number of azo bonds the longer the degradation process (Anku *et al.*, 2016).

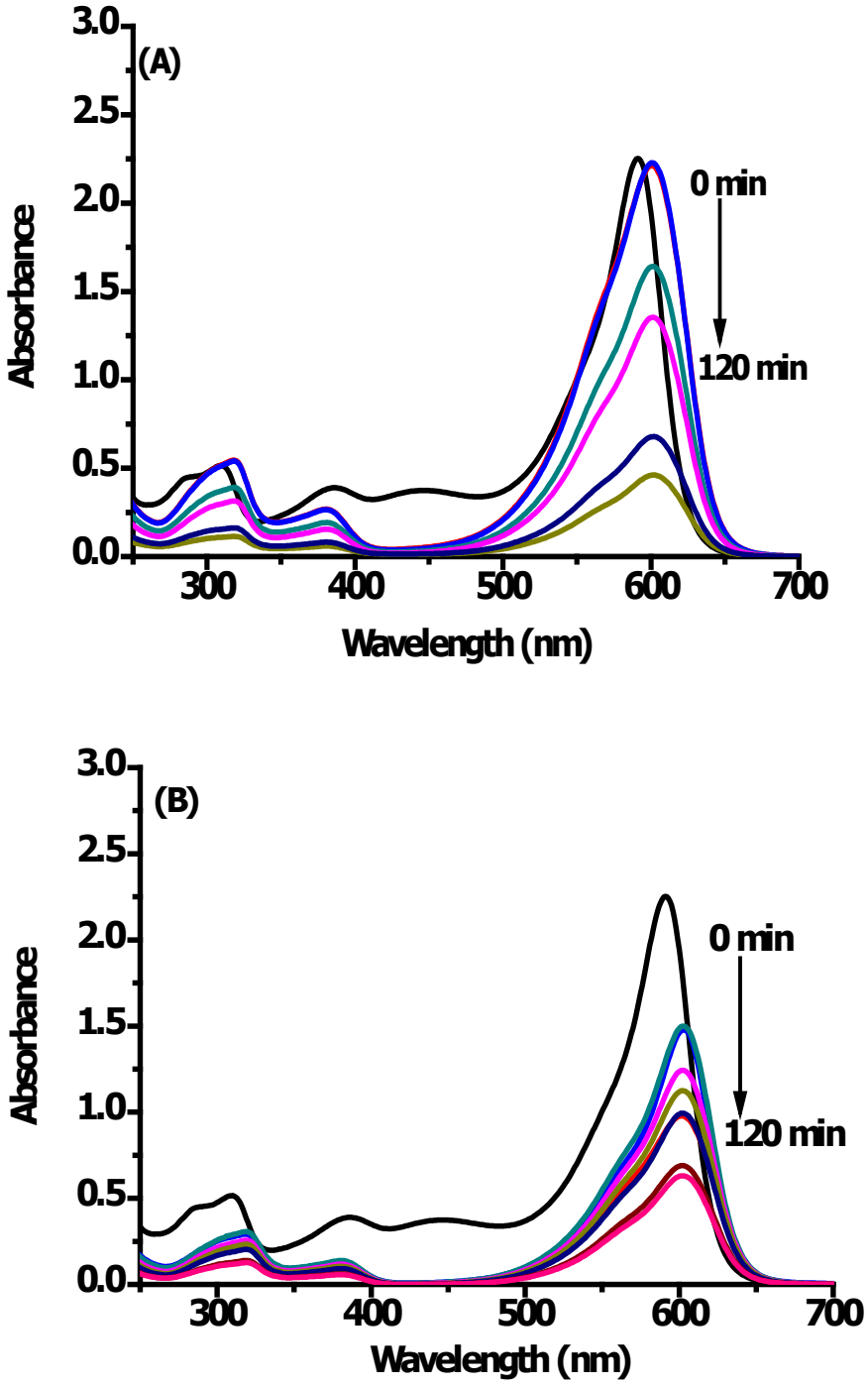

Figure 4.1: UV-Visible spectra for degradation of CR using (A) (AuNRs/TiO_2) and (B) (AuNS/TiO_2).

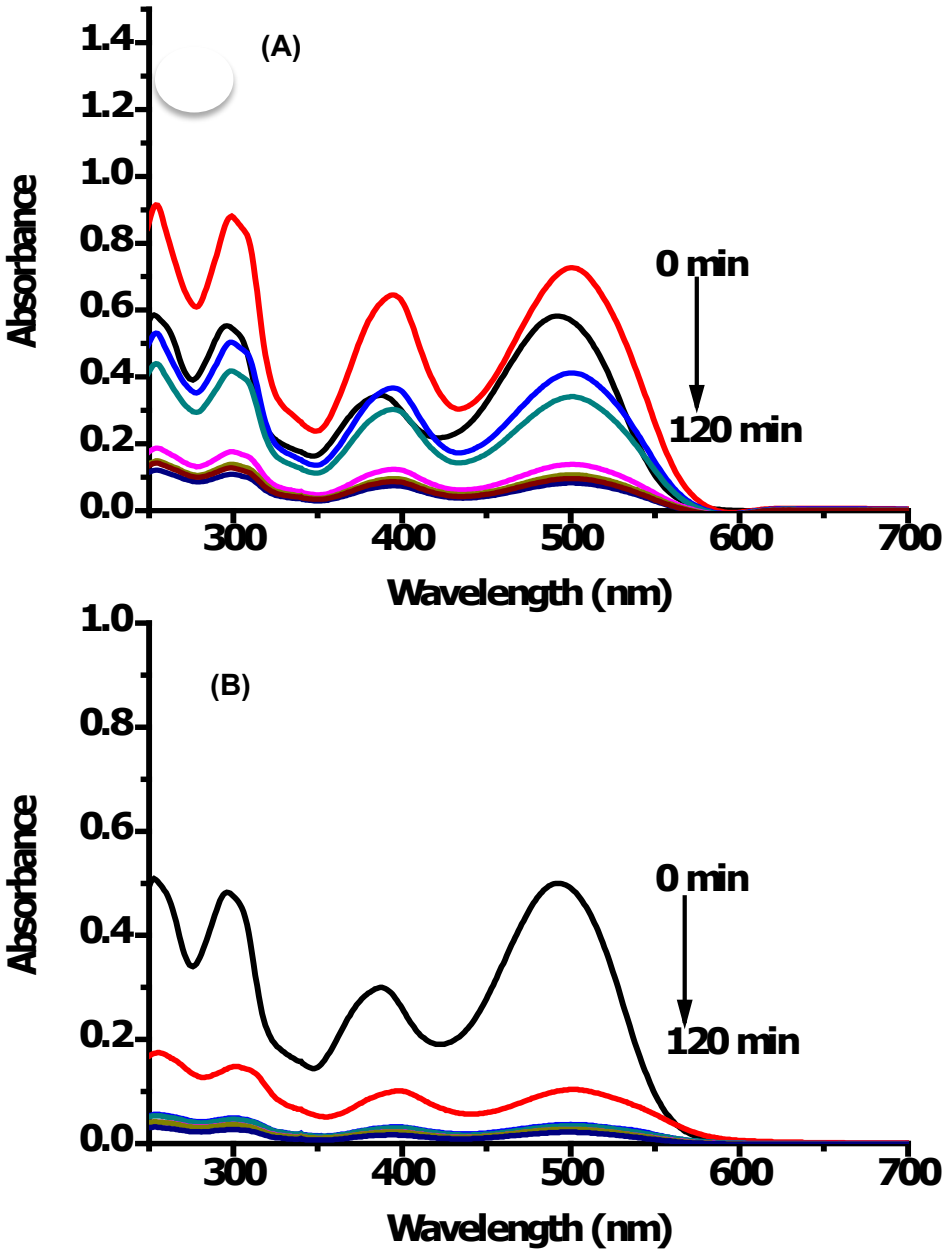

Figure 4.2: UV-Visible spectra for degradation of RO 16 using (A) ($AuNRs/TiO_{2)}$ and (B) ($AuNS/TiO_2$).

The first-order Langmuir-Hinshelwood kinetic model was used to evaluate the rate constants for the kinetic degradation on CR and RO 16 in presence of Au/TiO_2 nanocomposites. The kinetics of catalytic degradation of CR and RO 16, catalysed by $AuNS/TiO_2$ nanocomposites and $AuNRs/TiO_2$ are presented in **Figure 4.3**. The first-order rate constants (k) were obtained according to the following equation:

$$\ln\left(\frac{C_0}{C}\right) = kt \qquad \textbf{(4.5)}$$

where C_0 and C are the reactant concentration at time t = 0 and t = t, respectively, and k is the reaction rate constant. The rate constants (k) were determined by linearity fitting the graphs. The first order rate constants are presented in **Table 4.1**. The obtained rate constants using AuNS/TiO_2 photocatalyst were 0.0056 min^{-1} and 0.0483 min^{-1} for the degradation of CR and RO 16, respectively. When using AuNRs/TiO_2, the obtained rate values were 0.0031 min^{-1} and 0.0073 min^{-1} for CR and RO 16, respectively. Compared to CR, RO 16 was degraded faster by both catalysts.

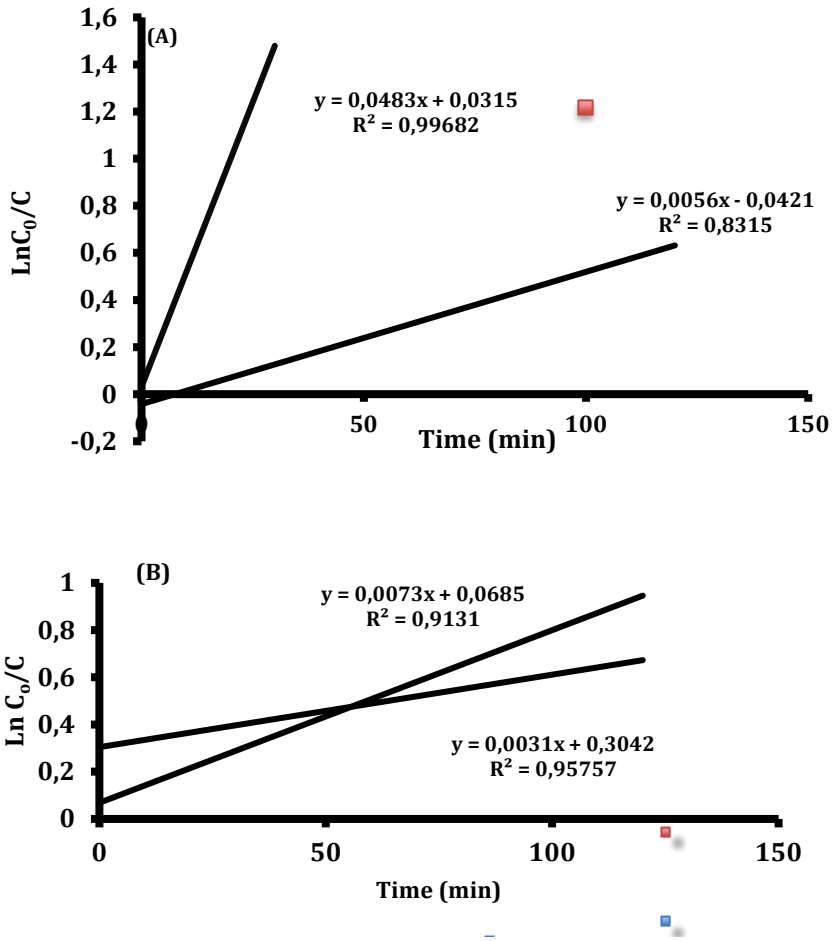

Figure 4.3: Pseudo-first order kinetic fits for the degradation of CR and RO 16, (A) catalysed by AuNS/TiO_2 nanocomposites and (B) catalysed by AuNRs/TiO_2.

The photocatalytic degradation efficiency of the composite catalysts (AuNS/TiO_2 and AuNRs/TiO_2) for the removal of CR and RO 16 under visible light were evaluated, and the results are shown in **Table 4.1** and **Figure 4.4.** The presence of gold nanoparticles in the photocatalysts prompted the photocatalytic activity under visible light. The dye solutions were stirred in the dark in the presence of the photocatalyst for 10 mins to allow adsorption-desorption process to take place. Pre-adsorption of dyes on the surface of the photocatalysts is crucial, since photocatalysis takes place on the surface. AuNS/TiO_2 demonstrated high adsorption of the dyes in the first

10 mins due to the presence of the small spherical particles. A degradation efficiency of 79.2% and 83.1% was achieved for CR using AuNS/TiO_2 and AuNRsTiO_2, respectively. For the degradation of RO 16, the AuNS/TiO_2 photocatalyst resulted in 91.4% degradation efficiency while the AuNRs/TiO_2 photocatalyst achieved 87% degradation efficiency after irradiating for 120 min. Due to the higher adsorbing property of the AuNS/TiO_2, higher removal efficiency was achieved for the removal of the RO 16 (monoazo) dye. However, for the diazo dye (CR) the adsorption process was reduced due to the bigger size of this dye compared to the mono azo dye (RO 16). The photocatalytic efficiency increased in the order of AuNRs/TiO_2 > AuNS/TiO_2 in both dye solutions.

The results show that the incorporated gold nanoparticles are able to produce hot electrons under visible light, which in turn were transferred to the conduction band of the TiO_2. Based on the results obtained, the shape of the gold nanoparticles in the composites had a great influence on the behaviour of the photocatalysts. It can be seen that the photocatalyst containing gold nanorods achieved higher photocatalytic degradation efficiency compared to the one with the spherical particles. The higher photocatalytic degradation efficiency is due to the contribution of two distinct transverse and longitudinal plasmon peaks of the gold nanorods, which enhances light absorption from a broader spectrum. This results are similar to the one achieved by (Kowalska, Abe and Ohtani, 2009). Additionally, incorporation of Au nanoparticles plays an important role in promoting visible light photocatalytic activity suggesting a smooth electron transfer between titania and Au. The electric energy per order was also calculated for photocatalytic process using the two photocatalysts. The values of the calculated E_{EO} are given in **Table 4.1**. Compared to CR, the degradation of RO 16 gave lower E_{EO} values. The lower E_{EO} values were due to faster degradation process for this dye.

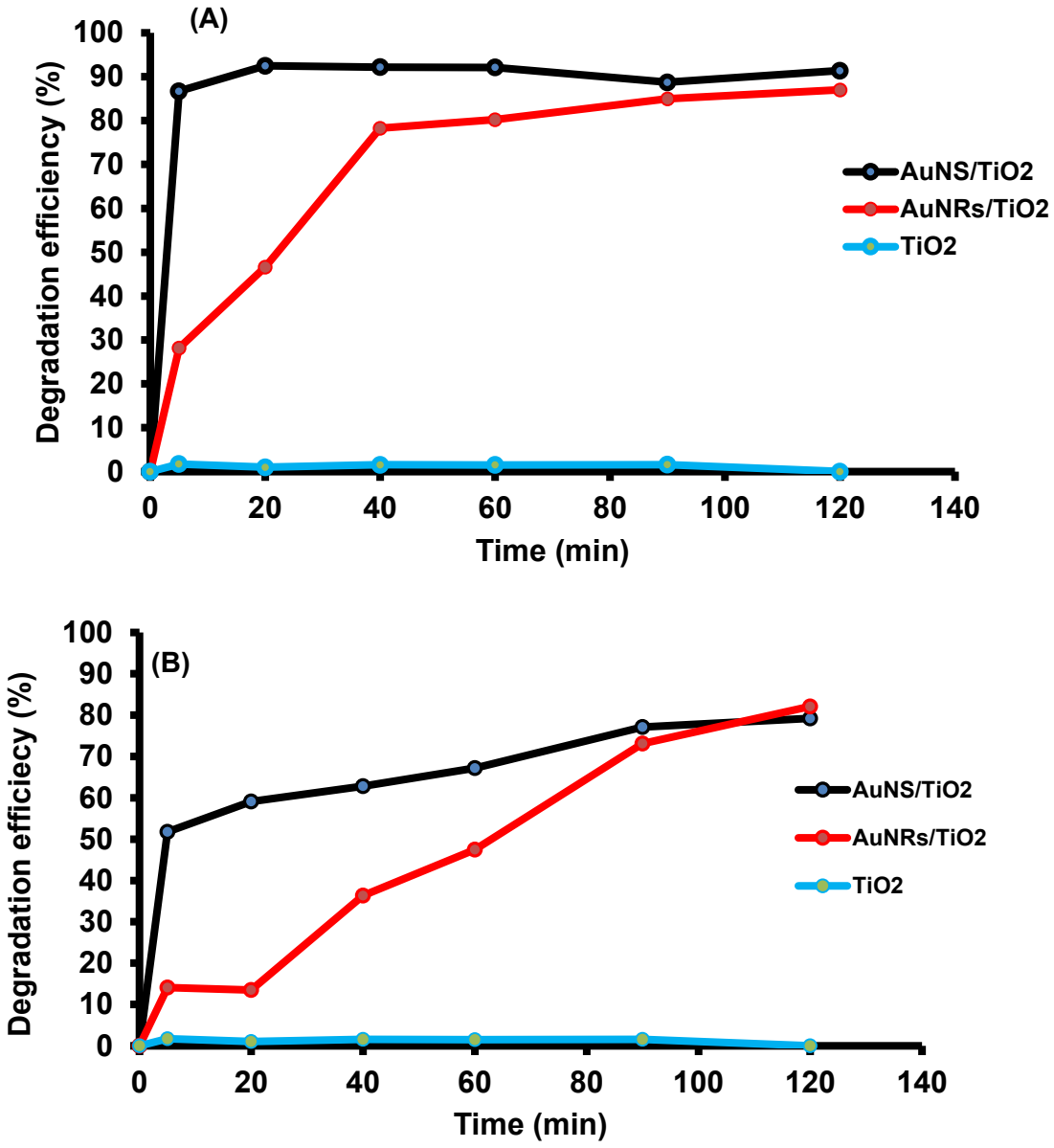

Figure 4.4: Degradation efficiency for and as a function of time using (A) RO 16 and (B) CR using AuNS/TiO_2,AuNRs/TiO_2andTiO_2).

Table 4.1: Photodegradation and kinetic properties of CR and RO16 using the Au/TiO_2 composites.

Catalyst	Dye	Efficiency (%)	K (min^{-1})	R^2	E_{EO} (kWh/m^3)
$AuNS/TiO_2$	CR	79.2	0.0056	0.832	8229
	RO 16	91.4	0.048	0.997	954
$AuNRs/TiO_2$	CR	83.1	0.0031	0.958	14864
	RO 16	87	0.0073	0.913	5961

4.5. Photocatalysis under direct sunlight

Utilizing direct sunlight to drive photocatalytic treatment of wastewater is a desired option in this field. Gold nanoparticles have been recognized as suitable materials for harvesting light of a broad spectrum due to their strong surface plasmon characteristic. In this study, two model azo dyes (CR and RO 16) were degraded as under solar light irradiation. Experiments were carried out during December, 2018. Solar irradiation experiments were performed in an open atmosphere between 11.00 a.m.-2.00 p.m. Sunlight illuminations was accomplished in a 500 cm^3 glass container containing 250 cm^3 of the dye solution. Aliquots were extracted from the reaction at specified time intervals. The photocatalytic degradation of CR and RO 16 was studied using $AuNRs/TiO_2$ as a photocatalyst under the sun. The obtained results are illustrated in **Figure 4.5**. UV-Vis spectra analysis shows the photocatalytic degradation process of the two dyes under the sun. In the presence of sunlight complete degradation of dyes was achieved in 180 min. The obtained degradation efficiencies were 99.9% and 99.8% for the degradation of RO 16 and CR, respectively. The results confirm the design of solar light active responsive Au/TiO_2 photocatalyst. The rate constants for pseudo-first-order kinetics were 0.0339 min^{-1} and 0.0367 min^{-1} for the photodegradation of CR and RO 16, respectively. Compared to visible light, the results showed that efficiency of dye degradation is better when photodegradation was performed under solar light. This work shows that the Au/TiO_2 plasmon enhanced photocatalyst are highly promising materials for applications towards degradation of textile dyes under direct sunlight.

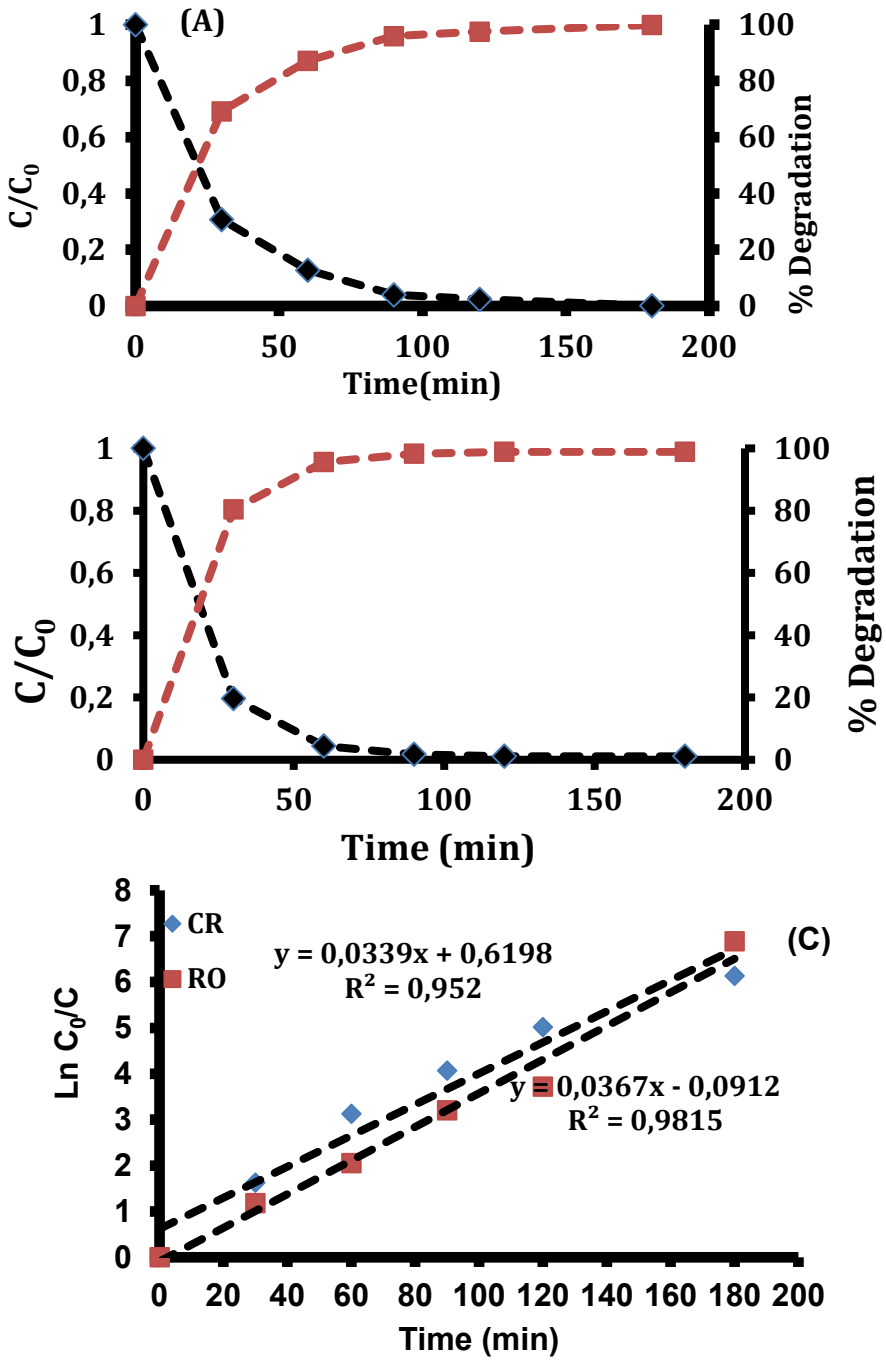

Figure 4.5: Change in concentration and degradation efficiency graphs for the degradation of (A) CR and (B) RO 16. (C) Pseudo-first order kinetic fits for the degradation CR 16 and RO 16.

4.6. Photocatalyst Regeneration

The recycling of powder heterogeneous photocatalysts is very important in the field of photocatalysis as it determines the stability of the catalyst. An ideal photocatalyst is the one that can be easily recycled and reuse after each experiment, it should not lose its catalytic properties after usage (Padikkaparambil et al., 2013). To evaluate the reusability of AuNRs/TiO_2, the

photocatalyst was separated from the reaction mixtures by centrifugation and used under the same conditions. The achieved photodegradation efficiencies were 86.6%, 85.8%, 85.2% and 79.9%, for the first, second, third, and forth cycles, respectively **(Figure 4.6**). As it can be seen from these values, the photocatalyst showed good stability without any significant loss. However, the decrease in the efficiency after the forth cycle maybe be due to the agglomeration of the dye molecules on the photocatalyst surface, which reduces the adsorption of the new dye molecules in the solution.

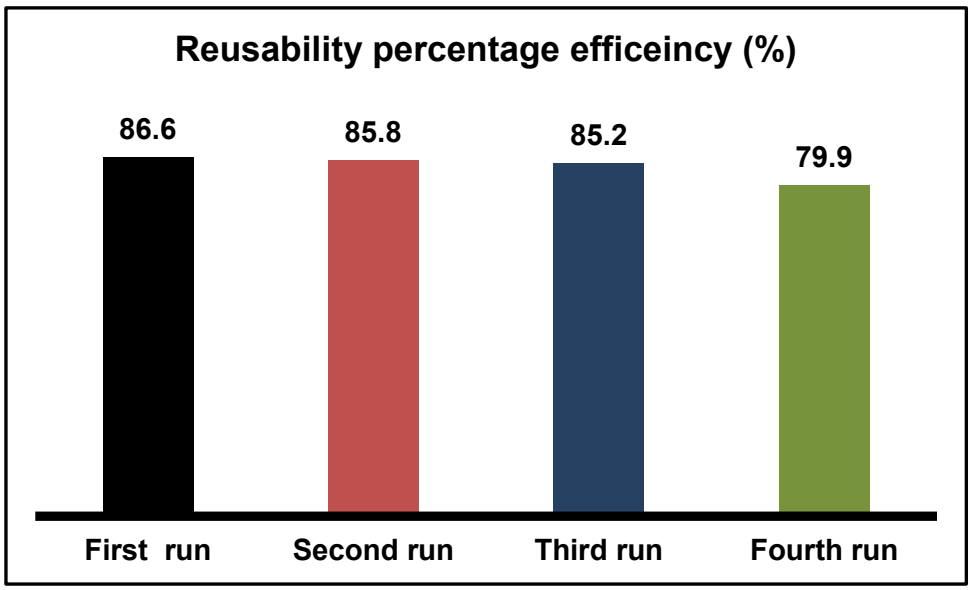

Figure 4.6: Cyclic photocatalytic degradation of azo dyes using Au/TiO_2 photocatalyst

4.7. Conclusion

Solar photocatalysis has the potential to utilize the most abundant energy to overcome the pressing issues related to water. The main problem to the realization of solar photocatalytic wastewater treatment is the limited absorption in the visible spectrum. Therefore, in this study, the photocatalytic activity of TiO_2 was improved by combining with the surface plasmon gold nanoparticles. Visible light illumination excites the plasmon hot electron of the gold nanoparticles which can be transferred to the conduction band of the TiO_2, and then facilitate the photocatalytic reaction. In this work, gold nanoparticles have shown significant promise in facilitating visible light photo-response in TiO_2 for photocatalytic degradation of azo dyes. The results show excellent photocatalytic efficiency for the degradation of azo dyes in water by plasmon photocatalysts. Moreover, the photocatalyst exhibit good stability for recycling and re-use. Due to the absorption of visible light of a broader range by gold nanorods, the AuNRs/TiO_2 showed higher photocatalytic activity. The AuNS/TiO_2 demonstrated adsorbing properties owing to the large surface area of the spherical nanoparticles. The Au/TiO2 photocatalyst shows highly promising results under natural sunlight for the degradation of azo dyes.

CHAPTER 5

CONCLUSIONS AND RECOMMENDATIONS

In summary, the synthesis and the properties of the plasmonic photocatalysts have been discussed. The photocatalysts presented in this work were constructed by incorporating spherical (AuNS) and rod-like gold nanostructures (AuNRs) into TIO_2. These photocatalysts were represented as AuNS/TiO_2 and AuNRs/TiO_2, respectively.

These photocatalysts have been used for the degradation two selected azo dyes (Congo red and reactive orange 16) in a slurry reactor. Incorporating gold nanoparticles into TiO_2 improved its photo-response in the visible spectrum. The visible light activity of Au/TiO_2 compared to TiO_2 alone can be explained by the enhanced light absorption by gold nanoparticles and the formation of schottky barrier junctions between the metal nanoparticles and the TiO_2.

The photodegradation process of RO 16 was faster than that of CR, and this was because CR has two azo groups. AuNS/TiO_2 demonstrated higher absorption due to the present of small particles of isotropic nature. However, AuNRs/TiO_2 photocatalyst presented higher photodegradation efficiency for CR compared to AuNS/TiO_2, this was due to the stronger magnetic field created by nanorods as a result of the photon absorption from both the transverse and longitudinal peaks.

Photodegradation process correlated with pseudo-first-order kinetic model for both dyes. Moreover, the results showed colour removal during photodegradation. The electric energy per order was found to increase as the number of the azo groups on the dye structure increases. Moreover, it was also observed that the process the photocatalyst can be reused without significant loss in activity. This photocatalyst can also be used towards photocatalytic degradation of the textile dyes under direct sunlight.

Recommendations

Photodegradation of textile azo dyes using plasmon enhanced TiO_2 photocatalyst has presented promising results for effective use of solar energy in wastewater treatment. In our view, the future research in this field may be dedicated on the following aspects:

- Firstly, more effort should be directed towards finding simple method for the production of photocatalysts at a large scale.
- Future research should also be focus on real wastewater and optimization of process parameters including: light absorption and distribution, charge and energy transfer kinetics.
- Studies on the effect of photocatalysis on the wastewater disinfection, and especially if this process is used in combination with a biological process.
- Additionally, the design of the efficient solar reactors that will allow effective light absorption by the photocatalyst requires attention.

REFERENCES

Access, O. (2018) 'We are IntechOpen , the world ' s leading publisher of Open Access books Built by scientists, for scientists TOP 1%', *Long-Haul Travel Motivation by International Tourist to Penang*, i(tourism), p. 13.

Akouibaa, A., Benhamou, M. and Derouiche, A. (2013) 'Simulation of the Optical Properties of Gold Nanorods : Comparison to Experiment', *International Journal of Advanced Research in Computer Science and Software Engineering*, 3(9), pp. 657-671.

Ananthashankar, A.G. (2014) 'Production, Characterization and Treatment of Textile Effluents: A Critical Review', *Journal of Chemical Engineering & Process Technology*, 05(01), pp. 1-18.

Anku, W.W. *et al.* (2016) 'Comparative photocatalytic degradation of monoazo and diazo dyes under simulated visible light using Fe3+/C/S doped-TiO_2 nanoparticles', *Acta Chimica Slovenica*, 63(2), pp. 380-391.

Atul, W. *et al.* (2013) 'Removal of organic pollutant from water by heterogeneous photocatalysis: a review', *Res J Chem Environ*, 17(September), pp. 84-94.

Bafana, A., Devi, S.S. and Chakrabarti, T. (2011) 'Azo dyes: past, present and the future', *Environmental Reviews*, 19(NA), pp. 350-371.

Barakat, M.A. *et al.* (2014) 'Pt nanoparticles/TiO2 for photocatalytic degradation of phenols in wastewater.' *Environmental technology*, 35(1-4), pp. 137-44.

Baruah, S., Pal, S.K. and Dutta, J. (2012) 'Nanostructured Zinc Oxide for Water Treatment', *Nanoscience and Technology-Asia*, 2(2), pp. 90-102.

Benkhaya, S., Harfi, S. El and Harfi, A. El (2017) 'Classifications, properties and applications of textile dyes: A review', *Applied Journal of Environmental Engineering Science*, 3(March 2018), pp. 311-320.

Bolton, J.R. *et al.* (2001) 'Figures-of-merit for the technical development and application of advanced oxidation technologies for both electric- and solar-driven systems (IUPAC Technical Report)', *Pure and Applied Chemistry*, 73(4), pp. 627-637.

Chen, Y. *et al.* (2015) 'Efficient degradation of methylene blue over two-dimensional Au/TiO<inf>2</inf> nanosheet films with overlapped light harvesting nanostructures', *Journal of Nanomaterials*, 2015(December).

Cheng, Y. *et al.* (2016) 'Surface plasmon resonance enhanced visible-light-driven photocatalytic activity in Cu nanoparticles covered Cu2O microspheres for degrading organic pollutants', *Applied Surface Science*. Elsevier B.V., 366, pp. 120-128.

D'Arienzo, M. *et al.* (2011) 'Photogenerated defects in shape-controlled TiO_2 anatase nanocrystals: A probe to evaluate the role of crystal facets in photocatalytic processes', *Journal of the American Chemical Society*, 133(44), pp. 17652-17661.

Designing, A. (2016) 'Decolourization of textile dye effluents', 3, pp. 22-30.

Goi, A. (2005) 'Advanced Oxidation Processes for Water', (June 1996), pp. 1-83.

Gravelet-Blondin, L.R. *et al.* (1997) 'Management of water resources in South Africa with respect to the textile industry', *Water Science and Technology*. International Association on Water Quality, 36(2-3), pp. 303-310.

Gupta, S. and Tripathi, M. (2012) 'A review on the synthesis of TiO_2 nanoparticles by solution route', *Open Chemistry*, 10(2).

Han, X. *et al.* (2009) 'Synthesis of Titania Nanosheets with a High Percentage of Exposed (001) Facets and Related Photocatalytic Properties Synthesis of Titania Nanosheets with a High Percentage of Exposed (001)', *Society*, (001), pp. 1-3.

Holkar, C.R. *et al.* (2016) 'A critical review on textile wastewater treatments: Possible approaches', *Journal of Environmental Management*. Elsevier Ltd, 182, pp. 351-366.

Hou, W. and Cronin, S. B. (2013) 'FEATURE ARTICLE A Review of Surface Plasmon Resonance-Enhanced Photocatalysis', pp. 1612-1619.

Jiao, Y. *et al.* (2015) 'Schottky barrier formation and band bending revealed by first-principles calculations', *Scientific Reports*, 5.

Khan, M.R. *et al.* (2015) 'Schottky barrier and surface plasmonic resonance phenomena towards the photocatalytic reaction: Study of them. Catalysis Science & Technology', *Catalysis Science & Technology*. Royal Society of Chemistry, (January).

Kowalska, E., Abe, R. and Ohtani, B. (2009) 'Visible light-induced photocatalytic reaction of gold-modified titanium(IV) oxide particles: Action spectrum analysis', *Chemical Communications*, (2), pp. 241-243.

Lan, Y.C., Lu, Y.L. and Ren, Z.F. (2013) 'Mini review on photocatalysis of titanium dioxide nanoparticles and their solar applications', *Nano Energy*, 2(5), pp. 1031-1045.

Li, B. *et al.* (2014) '(Gold Core) @(Ceria Shell) Nanostructures for Plasmon-Enhanced Catalytic Reactions under Visible Light', *ACS Nano*, 8(8), pp. 8152-8162.

Liu, G. *et al.* (2011) 'ChemComm Crystal facet engineering of semiconductor photocatalysts : motivations, advances and unique properties', pp. 6763-6783.

Liu, L. *et al.* (2015) 'Growth of nano Ag@AgCl on (111) facets of Cu_2O microcrystals with an enhanced photocatalytic activity', *RSC Adv.* Royal Society of Chemistry, 5(76), pp. 62306-62313.

Liu, S., Yu, J. and Jaroniec, M. (2010) 'Tunable Photocatalytic Selectivity of Hollow TiO_2 Microspheres Composed', *Society*, pp. 1-9.

Liu, Y., Wei, S. and Gao, W. (2015) 'Ag/ZnO heterostructures and their photocatalytic activity under visible light: Effect of reducing medium', *Journal of Hazardous Materials*. Elsevier B.V., 287, pp. 59-68.

Ma, X.Y. *et al.* (2010) 'Fabrication of uniform anatase TiO_2 particles exposed by {001} facets.' *Chemical communications (Cambridge, England)*, 46(35), pp. 6608-6610

McMullan, G. *et al.* (2001) 'Microbial decolourisation and degradation of textile dyes', *Applied Microbiology and Biotechnology*, 56(1-2), pp. 81-87.

Mondal, K. and Sharma, A. (2016) 'Recent advances in the synthesis and application of photocatalytic metal-metal oxide core-shell nanoparticles for environmental remediation and their recycling process', *RSC Adv.* Royal Society of Chemistry, 6(87), pp. 83589-83612.

Munirah, S. *et al.* (2018) 'A review on methods of synthesizing nanostructures TiO_2', *AIP Conference Proceedings*, 1963.

Nidheesh, P.V., Zhou, M. and Oturan, M.A. (2018) 'An overview on the removal of synthetic dyes from water by electrochemical advanced oxidation processes', *Chemosphere*, 197, pp. 210-227.

Ohno, T., Sarukawa, K. and Matsumura, M. (2002) 'Crystal faces of rutile and anatase TiO_2 particles and their roles in photocatalytic reactions', *New Journal of Chemistry*, 26(9), pp. 1167-1170.

Oke, N. (2018) 'Effluent Management in Textile Industry', 2(3), pp. 2-4.

Pattanaik, P. and Sahoo, M.K. (2013) 'TiO_2 photocatalysis: progress from fundamentals to modification technology', *Desalination and Water Treatment*, 52(34-36), pp. 6567-6590.

Pelaez, M. *et al.* (2012) 'A review on the visible light active titanium dioxide photocatalysts for environmental applications', *Applied Catalysis B: Environmental*. Elsevier B.V., 125, pp. 331-349.

Rahim Pouran, S., Abdul Aziz, A.R. and Wan Daud, W.M.A. (2015) 'Review on the main advances in Photo-Fenton oxidation system for recalcitrant wastewaters', *Journal of Industrial and Engineering Chemistry*. The Korean Society of Industrial and Engineering Chemistry, 21, pp. 53-69.

Raji, J.R. and Palanivelu, K. (2011) 'Sunlight-induced photocatalytic degradation of organic pollutants by carbon-modified nanotitania with vegetable oil as precursor', *Industrial and Engineering Chemistry Research*, 50(6), pp. 3130-3138.

Samanta, K.K. *et al.* (2019) *Water consumption in textile processing and sustainable approaches for its conservation*, *Water in Textiles and Fashion*. Elsevier Ltd.

Sen, T.K. (2015) 'Review on Dye Removal from Its Aqueous Solution into Alternative Cost Effective and Non-Conventional Adsorbents', *Journal of Chemical and Process Engineering*, 1.

Shah, Z.H. *et al.* (2015) 'Highly enhanced plasmonic photocatalytic activity of $Ag/AgCl/TiO_2$ by CuO co-catalyst', *J. Mater. Chem. A*, 3(7), pp. 3568-3575.

Shireesha *et al.* (2017) 'A Review on Effluent Treatment of Textile by Biological and Chemical Methods', *International Journal of Engineering Technology Science and Research*, 4(11), pp. 2394-3386.

Singh, K. and Arora, S. (2011) 'Removal of Synthetic Textile Dyes from Wastewaters: A Critical Review on Present Treatment Technologies', *Critical Reviews in Environmental Science and Technology*, 41(9), pp. 807-878.

Stasinakis, A.S. (2008) 'Use of Selected AOPs for Wastewater Treatment – A Mini-Review', *Global NEST Journal*, 10(3), pp. 376-385.

Sun, Yiqiang *et al.* (2016) 'Liu, L., Lin, S., Hu, J., Liang, Y. and Cui, W., 2015. Growth of nano Ag@AgCl on (111) facets of Cu_2O microcrystals with an enhanced photocatalytic activity. RSC Advances, 5(76), pp.62306-62313.', *Nanoscale*, pp. 5-8.

Tanveer, M. and Tezcanli Guyer, G. (2013) 'Solar assisted photo degradation of wastewater by compound parabolic collectors: Review of design and operational parameters', *Renewable and Sustainable Energy Reviews*. Elsevier, 24, pp. 534-543.

Tran, M. *et al.* (2016) 'Effect of citrate ratio and temperature on gold nanoparticle size and morphology Effect of citrate ratio and temperature on gold nanoparticle size and morphology'.

Vinu, R., Akki, S.U. and Madras, G. (2010) 'Investigation of dye functional group on the photocatalytic degradation of dyes by nano-TiO_2', *Journal of Hazardous Materials*, 176(1-3), pp. 765-773.

Vlok, E. (2006) 'Textile and Clothing Industry in Sub-Saharan Africa', *Friedich-Ebert-Stiftung*, pp. 227-246.

Wang, Y. *et al.* (2016) 'Size Control and Growth Process Study of Au@Cu_2O Particles', *Nanoscale Research Letters*. Nanoscale Research Letters, 11(1), p. 390.

Willets, K.A. and Van Duyne, R.P. (2007) 'Localized Surface Plasmon Resonance Spectroscopy and Sensing', *Annual Review of Physical Chemistry*, 58(1), pp. 267-297.

Wu, W., Changzhong Jiang and Roy, V. a L. (2014) 'Recent progress in magnetic iron oxide-semiconductor composite nanomaterials as promising photocatalysts.', *Nanoscale*. Royal Society of Chemistry, 7(1), pp. 38-58.

Xiao, M. *et al.* (2013) 'Plasmon-enhanced chemical reactions', *Journal of Materials Chemistry A*, 1(19), p. 5790.

Ye, L. *et al.* (2013) 'The replacement of {101} by {010} facets inhibit the photocatalytic activity of anatase TiO_2', *Applied Catalysis B: Environmental*. Elsevier B.V., 134-135(August 2015), pp. 60-65.

Yuan, G. *et al.* (2015) 'Supporting Information Morphologically controllable synthesis of core-shell structured Au@ Cu_2O with enhanced photocatalytic activity', pp. 1-2.

Zhou, N. *et al.* (2013) 'TiO_2 coated Au/Ag nanorods with enhanced photocatalytic activity under visible light irradiation', *Nanoscale*, 5(10), p. 4236.

Zhou, N. *et al.* (2015) 'Plasmon-Enhanced Light Harvesting: Applications in Enhanced Photocatalysis, Photodynamic Therapy and Photovoltaics', *RSC Adv.*, (April 2016), pp. 29076-29097.